NASA TM X-187

TECHNICAL MEMORANDUM
X-187

STATIC AERODYNAMIC CHARACTERISTICS OF SEVERAL HYPERSONIC MISSILE-AND-CONTROL CONFIGURATIONS AT A MACH NUMBER OF 4.65

By James D. Church and Ida M. Kirkland

Langley Research Center
Langley Field, Va.

NATIONAL AERONAUTICS AND SPACE ADMINISTRATION

WASHINGTON

January 1960

NASA TM X-187

TECHNICAL MEMORANDUM
X-187

STATIC AERODYNAMIC CHARACTERISTICS OF SEVERAL HYPERSONIC MISSILE-AND-CONTROL CONFIGURATIONS AT A MACH NUMBER OF 4.65

By James D. Church and Ida M. Kirkland

Langley Research Center
Langley Field, Va.

NATIONAL AERONAUTICS AND SPACE ADMINISTRATION

WASHINGTON

January 1960

NATIONAL AERONAUTICS AND SPACE ADMINISTRATION

TECHNICAL MEMORANDUM X-187

STATIC AERODYNAMIC CHARACTERISTICS OF SEVERAL HYPERSONIC MISSILE-AND-CONTROL CONFIGURATIONS AT A MACH NUMBER OF 4.65*

By James D. Church and Ida M. Kirkland

SUMMARY

An investigation has been conducted in the Langley Unitary Plan wind tunnel to determine the stability and control characteristics at a Mach number of 4.65 of three basic hypersonic missile configurations incorporating cruciform arrangements, one having a body with delta fins and trailing-edge controls and two having a body with a flared skirt and two different sets of canard controls. The effect of center-of-gravity location on the trim characteristics in pitch of the various configurations is indicated. Longitudinal center-of-pressure location of the various models is presented, and the effect of the canard surfaces on the contributions of the flare is examined. The effectiveness of differential deflection of the controls in producing roll is illustrated along with the induced effects resulting from combined deflections.

INTRODUCTION

In order to avoid excessive heating rates, hypersonic missile configurations usually employ highly swept fins or body-mounted flares as aerodynamic stabilizing surfaces. Whether these types of surfaces are aerodynamically efficient enough to provide adequate maneuverability is subject to question, particularly for the type of missiles requiring large turning forces for maneuver, such as antimissile missiles, air-to-air interceptors, and so forth. Furthermore, these turning forces must generally be available at drag levels within the propulsion capabilities of systems designed to accelerate during these maneuvers.

In view of these problems, the National Aeronautics and Space Administration has undertaken an investigation of the stability and control characteristics of some general hypersonic missile configurations. Earlier results of this investigation, stability characteristics of several body-fin and body-flare geometries, are reported in references 1 (Mach number M, 2.01) and 2 (M = 2.29 to 4.65). As a continuation of the basic program, the control characteristics have been obtained for several configurations which represent modifications of the models tested in references 1 and 2. Some of the results of these more recent tests are contained in references 3 (M = 2.01, 4.65, and 6.8) and 4 (M = 6.8). The data obtained at M = 4.65 in the Langley Unitary Plan wind tunnel are reported herein. The three basic configurations examined in these later tests consisted of one model with a trailing-edge control in conjunction with a cruciform delta-fin arrangement and two flared-skirt models incorporating two different sets of canard arrangements.

The present tests were conducted over an angle-of-attack range from -1° to 21° and at angles of sideslip of about 0°, 4°, and 8°. Various pitch, roll, and yaw deflections were examined, and in one case, combined pitch and yaw deflections were tested. All data were obtained at M = 4.65 for a Reynolds number of 5.04×10^6 per foot. An analysis of the trimming ability of the various controls in pitch and the effect of the various configurations on longitudinal center-of-pressure location is presented herein. In addition, the aileron effectiveness and induced lateral characteristics of two of the models are compared.

An analysis of the trim characteristics, utilizing the data of reference 4 and some of the results of the present test, is presented in reference 5. This reference indicates the effect of Mach number on the pitch characteristics and also illustrates possible application of these configurations to the antimissile problem.

SYMBOLS

The basic data are presented as force and moment coefficients about a moment center located at 81.57 percent of the body length rearward of the nose. All data are referred to the body axes system shown in figure 1(a). In addition, a limited amount of the data is also referred to the stability axes system shown in figure 1(b).

C_A axial-force coefficient, $\frac{\text{Total axial force}}{qS} - C_{A,b}$

$C_{A,b}$ base axial-force coefficient, $\frac{\text{Base axial force}}{qS}$

C_D' drag coefficient, $C_A \cos \alpha + C_N \sin \alpha$

C_L lift coefficient, $C_N \cos \alpha - C_A \sin \alpha$

C_l rolling-moment coefficient, $\frac{\text{Rolling moment}}{qSd}$

$C_{l_\beta} = \frac{\partial C_l}{\partial \beta}$, per deg

$C_{l_{\delta_a}} = \frac{\partial C_l}{\partial \delta_a}$, per deg

C_m pitching-moment coefficient, $\frac{\text{Pitching moment}}{qSd}$

C_N normal-force coefficient, $\frac{\text{Normal force}}{qS}$

$C_{N_\alpha} = \frac{\partial C_N}{\partial \alpha}$, per deg

C_n yawing-moment coefficient, $\frac{\text{Yawing moment}}{qSd}$

$C_{n_\beta} = \frac{\partial C_n}{\partial \beta}$, per deg

$C_{n_{\delta_a}} = \frac{\partial C_n}{\partial \delta_a}$, per deg

C_Y side-force coefficient, $\frac{\text{Side force}}{qS}$

d diameter of cylindrical section of body, in.

L/D lift-drag ratio

l missile length, in.

M free-stream Mach number

q free-stream dynamic pressure, lb/sq ft

S cross-sectional area of cylindrical body, $\frac{\pi d^2}{4}$, sq ft

[redacted]

X,Y,Z orthogonal set of body axes

X_s,Y_s,Z_s orthogonal set of stability axes

x longitudinal distance rearward from nose measured along body center line, in.

α angle of attack referred to body center line, deg

β angle of sideslip referred to body center line, deg

δ control deflection, deg

δ_a roll control deflection from body center line, $(\delta_2 - \delta_4) + (\delta_3 - \delta_1)$, deg

$\frac{\partial \delta_a}{\partial \beta}$ ratio of aileron deflection to sideslip angle required to trim induced roll, $\frac{\partial C_l / \partial \beta}{\partial C_l / \partial \delta_a}$

δ_e pitch control deflection from body center line, $\frac{\delta_2 + \delta_4}{2}$, deg

δ_r yaw control deflection from body center line, $\frac{\delta_1 + \delta_3}{2}$, deg

Subscripts:

cg center of gravity

cp center of pressure

F flare in the presence of body

trim trimmed conditions

1,3 refers to top and bottom controls, respectively, (positive, trailing edge to left)

2,4 refers to right and left controls, respectively, (positive, trailing edge down)

[redacted]

APPARATUS AND MODELS

The tests were performed in the high Mach number test section of the Langley Unitary Plan wind tunnel. This tunnel is of the variable-pressure continuous-flow type with a test section 4 feet square and approximately 7 feet in length. Mach number may be varied continuously from approximately 2.3 to 4.7 by means of an asymmetric sliding-block nozzle.

Sketches of the configurations tested are presented in figure 2 and the geometric characteristics are given in table I. Photographs of two of the models are shown in figure 3. The basic body had a fineness ratio of 10, formed by equal-length forebodies and afterbodies. The forebody consisted of a rounded nose followed by a straight tapered section which faired into an ogive. This forebody, in turn, blended into the cylindrical afterbody. All fins and controls were flat plates with rounded leading edges and blunt trailing edges.

The cruciform-fin configuration will be referred to hereinafter as the model with delta fins and trailing-edge controls. This model had fins with 5° apex angles mounted in a cruciform arrangement on the basic body. Four trailing-edge flaps were located to the rear of the fins, the distance between the flaps and fins was 0.033 caliber. The flap hinge lines were at the 93.3-percent body station and 33.3-percent flap chord line.

The flared-afterbody configuration will be referred to herein as the model with flared skirt and large, or small, canard controls. This model had a 2-caliber 10° flared skirt mounted on the fuselage. Two sizes of modified, 70° delta, cruciform, all-moving canard surfaces were located at the 46.6-percent body station. Hinge-line locations in percent control root chord were 68.7 and 59.5 for the small and large canard surfaces, respectively.

Forces and moments for the model were measured by means of a six-component internal strain-gage balance. This balance was attached by means of a sting to the tunnel central support system. Included in the tunnel model support system was a remotely operated, adjustable angle coupling that permitted tests to be made at variable angles of attack concurrently with variations in the angle of sideslip.

[redacted]

TESTS, CORRECTIONS, AND ACCURACY

Tests

Tests were conducted for all configurations through an angle-of-attack range from -1° to 21° for an angle of sideslip of 0°. Yaw control effectiveness and the effects of sideslip on pitch effectiveness were determined from tests conducted over this angle-of-attack range at angles of sideslip of about 4° and 8°. Pitch control effectiveness was obtained with the use of deflections of 0°, -10.0°, -15.1°, and -20.0° for the trailing-edge flaps and 0°, 10.0°, and 20.0° for the canard controls. In addition, limited tests were conducted to evaluate the rudder and aileron control effectiveness. Only the trailing-edge controls utilized deflection of the rudder, and then in combination with a pitch deflection. For this test, all controls were set at 15.0° in a direction to trim simultaneously positive α and β. Aileron tests were made for both the trailing-edge and small canard controls. For the trailing-edge controls, all four surfaces were deflected 10.0° $\left(\delta_a = -40.0;\ \delta_e = \delta_r = 0^\circ\right)$; whereas, for the small canard surfaces only the two vertical controls were deflected 10.0° $\left(\delta_a = -20.0^\circ;\ \delta_e = \delta_r = 0^\circ\right)$. One test was conducted with the flared skirt removed in an attempt to determine the effect of the small canard surfaces on the flow over the afterbody.

All tests were conducted at a Mach number of 4.65 and a Reynolds number of 5.04×10^6 per foot of length. A stagnation pressure of about 13,360 pounds per square foot absolute, a dynamic pressure of approximately 578 pounds per square foot, and a stagnation temperature of 175° F were maintained through the tests.

Corrections and Accuracy

Corrections for tunnel flow misalinement and balance-sting deflection due to load have been applied to all the angles of attack and sideslip presented herein. In addition, all axial-force data have been adjusted to correspond to free-stream static pressure acting on the model base area including the area occupied by the sting. Pressures measured in the balance chamber and in the recessed base (including the flare when mounted) were applied to their individual areas to obtain this correction.

Possible errors in the presented data based on balance and tunnel calibration are as follows:

[redacted]

M	±0.02
α, β, deg	±0.2
δ_a, δ_e, δ_r, deg	±0.1
C_N, C_Y, C_L	±0.11
C_A, C_D'	±0.013
C_m, C_n	±0.13
C_l	±0.03

This table gives the accuracy of the absolute values of the quantities for use in evaluating the possible errors in isolated data. Experience indicates that the probable errors are about half this magnitude, particularly in determination of point-to-point variations. Furthermore, the basic data are presented about the balance moment center (0.8157l) in the same sequence that the tests were conducted. These results were then faired in a consistent manner before attempting any transfer to center-of-gravity locations of interest. It is believed that even though transfer arms of 30 percent of the body length are involved, the trim results are almost as accurate as the basic data. (See the section entitled "Discussion.")

PRESENTATION OF RESULTS

Typical schlieren photographs are presented in figure 4. Other results are presented as indicated in the following abbreviated outline:

[redacted]

DISCUSSION

The basic results of the investigation are presented about the balance moment center (0.8157l) rather than a more realistic center-of-gravity location, to avoid the inherent errors in mathematical transfer of raw moment data over large distances. These data were then faired in a consistent manner to remove any scatter and random out-of-trim moments due to balance zero shifts.

Longitudinal Characteristics

The pitch results are presented in the form of trim characteristics, as opposed to stability and control derivatives, to illustrate better the turning forces available for maneuver. In effect, this treats the three basic stabilizer-control combinations as complete systems. As a matter of interest, reference 3 contains some stability and control derivatives for a center-of-gravity location of 0.50l.

Trim characteristics.- The trim characteristics of the model with delta-fin with trailing-edge flaps were very nonlinear with control deflection (fig. 10(a)). In particular, values of the trimmed quantities per unit deflection increased with increasing deflection to $\delta_e = -15^\circ$ at all center-of-gravity positions illustrated. However, at $\delta_e = -20^\circ$ the configuration exhibited a loss in trim ability with respect to the -15° position independent of center-of-gravity position. The exact variation of the trim characteristics between these two values of δ_e is unknown; accordingly, dashed lines are used to indicate these variations. Regardless of the fairing employed, it is apparent that large losses in trim effectiveness per unit deflection occurred for values of δ_e greater than -15° (primarily as a result of a loss in control effectiveness).

Both of the canard configurations (figs. 10(b) and 10(c)) displayed trim characteristics that were relatively linear to $\delta_e = 20^\circ$, particularly for center-of-gravity locations between 0.50l and 0.55l. Furthermore, there was no evidence of losses in trim effectiveness per unit deflection for these models at any of the presented conditions.

The foregoing trim results are general and have been presented without regard to the possible application of the various configurations to some tactical mission. For purposes of further analysis, the results will be evaluated with the view that a mission is involved for which large turning forces are required. Figure 11 illustrates the trim characteristics (including L/D) as functions of center-of-gravity location

[redacted]

for an absolute value of control deflection of 15°. In each case, the curves have been terminated at the rearward center-of-gravity locations at which neutral stability occurred. Consequently, the magnitudes of the quantities shown in this figure correspond to the largest values trimmable ($|\delta_e| = 15.0°$) without encountering the region of reversal in trim per unit deflection exhibited by the trailing-edge controls (dashed portion of curves in fig. 10(a)).

The angle-of-attack variations shown in figure 11 are of interest only to indicate the attitude required of each of the configurations to develop the turning forces shown in the upper portion of this figure. These results indicate that the canard surfaces were much more effective than the trailing-edge controls when considered from an ability to produce lift. This condition is particularly evident when it is recalled that no losses in trim per unit deflection occurred for the canard surfaces even at the larger δ_e values. In fact, a value of δ_e of 20.0° produces $C_{N,trim}$ values of 5 and 7 for the small and large canard surfaces, respectively, at the most rearward center-of-gravity location (figs. 10(b) and 10(c)).

It should be noted, however, that this increase in maneuverability for the canard surfaces would be achieved with some attendant drag penalty, as compared with that of the trailing-edge controls, if thrust-off operation were contemplated. This penalty arises from a decrease in L/D levels presented for the canard—flared-skirt geometries as a consequence of the larger base pressures acting on the base and flare with power off (L/D values in fig. 11 correspond to free-stream pressure acting on the base). Of course, this analysis presupposes that a flare will be used as the stabilizing device for the canard configuration. Use of an alternate device such as jet reaction would eliminate this L/D loss due to power-off operation.

In reference 5, the following criterion is given: C_L values on the order of 2 to 3 are required for maneuver performance in the antimissile problem. Hence, the data of figure 11 suggest that all the reported configurations might have application in this category if the missile were designed to operate up to a Mach number of 4.65. Furthermore, both the maximum $C_{N,trim}$ and the Mach number at which appreciable losses in effectiveness occur could probably be increased by interdigitating suitable combinations of the tested controls and stabilizing surfaces. (See, e.g., ref. 6.)

Center of pressure.- The travel of the longitudinal center-of-pressure locations with angle of attack for the various configurations is illustrated in figure 12. Also shown are the applicable results for similar configurations without controls which were reported in

reference 2. The dashed portions of the curves at the lower α values represent center-of-pressure values determined by slopes (corresponding to aerodynamic center at $\alpha = 0^\circ$); the use of slopes was necessitated by the small magnitude of C_m that existed at these values of α.

Incorporation of the trailing-edge flaps with the finned configuration of reference 2 resulted in a small rearward center-of-pressure shift. This movement is opposite to what would be anticipated as a result of the small reduction in area of the present model with respect to that of the reference. At least half of the center-of-pressure movement can be attributed to the repeatability of the accuracy of the two tests ($0.01l$ corresponds to only 0.3 inch of model length). It is believed that the remainder of this rearward shift can be attributed to the effect of the gap between the fins and controls, at least at the larger values of α. Differences between the results of the reference and those for the small canard surface of the present test, however, reflect the canard-surface wake effects on the flared afterbody. This latter effect will be discussed in greater detail subsequently.

As might have been expected, a control deflection of 10° (in a direction of trim positive values of α) resulted in forward center-of-pressure shifts on the order of $0.02l$ to $0.04l$ for all configurations of the present investigation. Furthermore, at $\delta_e = 0^\circ$, all geometries had center-of-pressure locations between $0.58l$ and $0.62l$ for the presented range of angle of attack of 0° to 21°. It is of interest to note that the center-of-pressure travel of the two canard configurations (for $\alpha > 8^\circ$) was substantially the same (within $0.01l$) at either of the two values of δ_e tested despite the 22-percent difference in control areas.

Flared-skirt effects.- The characteristics of the flared skirt, considered as an isolated body but including the interference effects of the fuselage and canard, are presented in figure 13. Normal-force contribution and center-of-pressure location of the isolated flared skirt with and without the presence of the small canard surfaces are illustrated. A value of C_{N_α} for the flare of about 0.050 per degree is essentially unaffected by the presence of the canard surfaces or the α range tested. On the other hand, some effect of the canard surfaces on the flare center-of-pressure location is indicated. The canard-off curve is seen to shift rearward until a value near the centroid of area is reached at $\alpha = 16^\circ$. This variation, as opposed to a constant location of two-thirds of the flare length, is probably attributable to three-dimensional considerations as well as to the blanketing effects of a shock-thickened boundary layer present at the lower values of α. The apparent rearward center-of-pressure shift due to the canard surfaces at low α is probably a result of further thickening due to the wake

of these surfaces of the boundary layer on the flare to such an extent that separation may have occurred.

Roll and Induced Characteristics

Aileron effectiveness.- The effects of differential deflection of the trailing-edge and small canard controls on the lateral characteristics of the models are shown in figure 14. An arbitrary center-of-gravity location of $0.55l$ was employed to provide some indication of the yaw properties. These results indicate that the canard surfaces are the better of the two systems when deflected in roll. The $C_{l_{\delta_a}}$ values, in fact, show that the canard surfaces were four to five times more effective over the α range tested. The canard superiority is further emphasized when it is recalled that only two controls in the vertical plane were differentially deflected for the canard-surface tests; whereas, the trailing-edge geometry utilized all four surfaces.

Induced characteristics.- It is recognized that control-induced cross coupling is basically dynamic in nature; consequently, static tendencies are at best only an indication of potential problem areas. Moreover, for missile designs of the type considered herein, the primary concern is to accomplish a prescribed maneuver (with allowances for gusts, thrust misalinements, etc.) without requiring control deflections in excess of the mechanical limits of practical servosystems (say in the range of 40°). Within this framework, a few interesting induced properties will now be presented which must be considered mainly as trends.

Effects of δ_a: The induced yaw characteristics due to aileron deflection are presented in figure 14(c). Since rudder-deflection tests were not performed for both models, little can be said regarding the δ_r requirements to trim the yawing-moment coefficients induced by δ_a other than that the absolute magnitudes of these induced yawing moments were about the same for both systems.

A second induced cross coupling is the tendency of the combination of $C_{n_{\delta_a}}$ and C_{l_β} (fig. 14(b)) to generate rolling moments that aid or resist the original C_l due to δ_a. For illustration, a negative value of δ_a would produce a positive value of C_l by virtue of a negative value of $C_{l_{\delta_a}}$, but this would in turn result in a positive value of C_n if $C_{n_{\delta_a}}$ is negative. Consequently, a missile would tend to yaw to a negative value of β, and if any of this negative value were not offset by the basic directional stability of the system, a negative

C_l would be induced by virtue of a positive C_{l_β}. This sequence of quasi-steady trends serves to illustrate that both of the controls of figure 14, when deflected as ailerons, would induce rolling moments in opposition to the intended aileron roll and thus reduce the effective $C_{l_{\delta_a}}$.

Effect of δ_e: Presented in figure 15 are some additional induced characteristics for the same configurations discussed previously. The parameter $\partial\delta_a/\partial\beta$ represents the aileron deflection per degree of yaw that would be required to trim the roll induced by the various pitch deflections. The crosshatched regions between the curves for the trailing-edge controls denotes the range of values of $\partial\delta_a/\partial\beta$ which are encompassed by 0° to 15° of pitch deflection. Implicit in these results is the $1\frac{1}{2}$-percent loss (per degree of β) in deflection range available if the system must trim the roll induced by virtue of trimming in pitch at a large value of α, say 15° ($|\delta_e| \approx 15°$). Although the trailing-edge controls exhibit little induced roll at low angles of attack, losses in available deflection range appear to exist to about the same degree for both configurations at the larger angles of attack.

Some insight into the possible causes of these induced properties is given in reference 7. This report presents results indicating the effects of all-movable-wing incidence on the induced rolling-moment characteristics of cruciform configurations. In this study, it was found that a deflected control directly in the path of a body vortex can be expected to produce large increments in induced rolling moment. Consequently, it is not surprising that configurations of the type tested might display induced characteristics where δ_e effects are noted on β derivatives and similarly δ_a or δ_r effects on α derivatives at combined α and β. Furthermore, the canard-surface areas are large enough with respect to the body cross-sectional area so that the control-on-control type of induced roll encountered with cruciform configurations might be anticipated. (See, e.g., C_l values in figs. 7(c) and 8(d) for $\beta \neq 0°$.)

As a further indication of the preceding induced effects, the effects of δ_e on the directional stability of the models are shown in figure 15; an arbitrary center-of-gravity location of $0.55l$ is again utilized. The rather large changes in C_{n_β}, at least for the canard model, illustrate the degree of cross coupling present for the type of configurations reported herein. All the induced characteristics presented indicate that certain problem areas may exist in utilizing the control systems reported herein. In the final analysis, a specific

design requiring explicit maneuvers would have to be employed to ascertain any dynamic problems that might result with any given servo design in conjunction with the reported control geometries.

CONCLUSIONS

An investigation has been made to determine the static stability and control characteristics at a Mach number of 4.65 of three basic hypersonic missile configurations with cruciform surfaces, one having a body with delta fins and trailing-edge controls and two having a body with a flared skirt and two different sets of canards.

1. The results indicate that the trailing-edge controls encountered severe losses in trim ability at deflections near -20° for all center-of-gravity positions examined (0.46 to 0.57 body length). Although all configurations produced about the same trim angles of attack for rearward center-of-gravity locations, the canard models provided substantial increases in trim lift. The trim characteristics of all geometries studied were very sensitive to center-of-gravity position as the neutral point was approached.

2. All configurations had center-of-pressure locations between 0.58l and 0.62l over the angle-of-attack range tested for zero deflection of the controls. A 22-percent reduction in canard area had little effect on either center-of-pressure location or trim independent of control deflection.

3. The contributions of the flared skirt to the aerodynamic characteristics of the basic body were only slightly affected by the presence of the canard surfaces.

4. The small canard surfaces were superior to the trailing-edge controls when used differentially as ailerons. However, both models, and in particular the canard configurations, exhibited induced roll and yaw characteristics which might in some instances present serious problems in any application to a particular missile servo design.

Langley Research Center,
National Aeronautics and Space Administration,
Langley Field, Va., August 26, 1959.

[redacted]

REFERENCES

1. Robinson, Ross B.: Wind-Tunnel Investigation at a Mach Number of 2.01 of the Aerodynamic Characteristics in Combined Angles of Attack and Sideslip of Several Hypersonic Missile Configurations With Various Canard Controls. NACA RM L58A21, 1958.

2. Turner, Kenneth L., and Appich, W. H., Jr.: Investigation of the Static Stability Characteristics of Five Hypersonic Missile Configurations at Mach Numbers From 2.29 to 4.65. NACA RM L58D04, 1958.

3. Spearman, M. Leroy, and Robinson, Ross B.: Longitudinal Stability and Control Characteristics at Mach Numbers of 2.01, 4.65, and 6.8 of Two Hypersonic Missile Configurations, One Having Low-Aspect-Ratio Cruciform Wings With Trailing-Edge Flaps and One Having a Flared Afterbody and All-Movable Controls. NASA TM X-46, 1959.

4. Robinson, Ross B., and Bernot, Peter T.: Aerodynamic Characteristics at a Mach Number of 6.8 of Two Hypersonic Missile Configurations, One With Low-Aspect-Ratio Cruciform Fins and Trailing-Edge Flaps and One With a Flared Afterbody and All-Movable Controls. NACA RM L58D24, 1958.

5. Stone, David G.: Maneuver Performance of Interceptor Missiles. NACA RM L58E02, 1958.

6. Winovich, Warren, and Higdon, Nancy S.: Evaluation of Some Aerodynamic Controls for a Low-Aspect-Ratio Missile. NACA RM A58D17b, 1958.

7. Mello, J. F., and Sivier, K. R.: Supersonic Induced Rolling Moment Characteristics of Cruciform Wing-Body Configurations at High Angles of Attack. Rep. 5642 (Contract No. NOrd-12826), McDonnell Aircraft Corp., Jan. 15, 1958.

[redacted]

[redacted]

TABLE I.- GEOMETRIC CHARACTERISTICS OF MODELS

Body:		
Length, in.		30.00
Diameter, in.		3.00
Maximum cross-sectional area, sq in.		7.07
Fineness ratio of nose		5.00
Length-diameter ratio, total		10.00
Moment-center location, percent length		81.57
Flare:		
Length, in.		6.01
Base diameter, in.		5.12
Base area, sq in.		20.58
Leading-edge angle, deg		10.00
Cruciform fins:		
Length (each), in.		16.02
Span (each), in.		1.34
Area, exposed (per pair), sq in.		20.92
Vertex angle, deg		5.00
Span-diameter ratio		1.89
Thickness, in.		0.19
Aspect ratio, exposed (per pair)		0.28
Trailing-edge flaps:		
Span, exposed (each), in.		1.34
Chord, in.		3.00
Area, per pair, sq in.		8.04
Hinge line, percent chord (from leading edge)		33.30
Hinge line, percent body length		93.30
Thickness, in.		0.19
Aspect ratio, exposed (per pair)		0.89
Canard control surface:	Small	Large
Span, exposed (each), in.	2.21	2.21
Span, diameter ratio	2.47	2.47
Leading-edge sweep angle, deg	70.00	70.00
Tip chord, in.	0.33	1.33
Root chord, in.	6.39	7.41
Area, exposed (per pair), sq in.	15.68	20.05
Hinge line, percent chord (from leading edge)	68.70	59.50
Hinge line, percent body length	46.60	46.60
Thickness, in.	0.19	0.19
Aspect ratio, exposed (per pair)	1.25	0.98

[redacted]

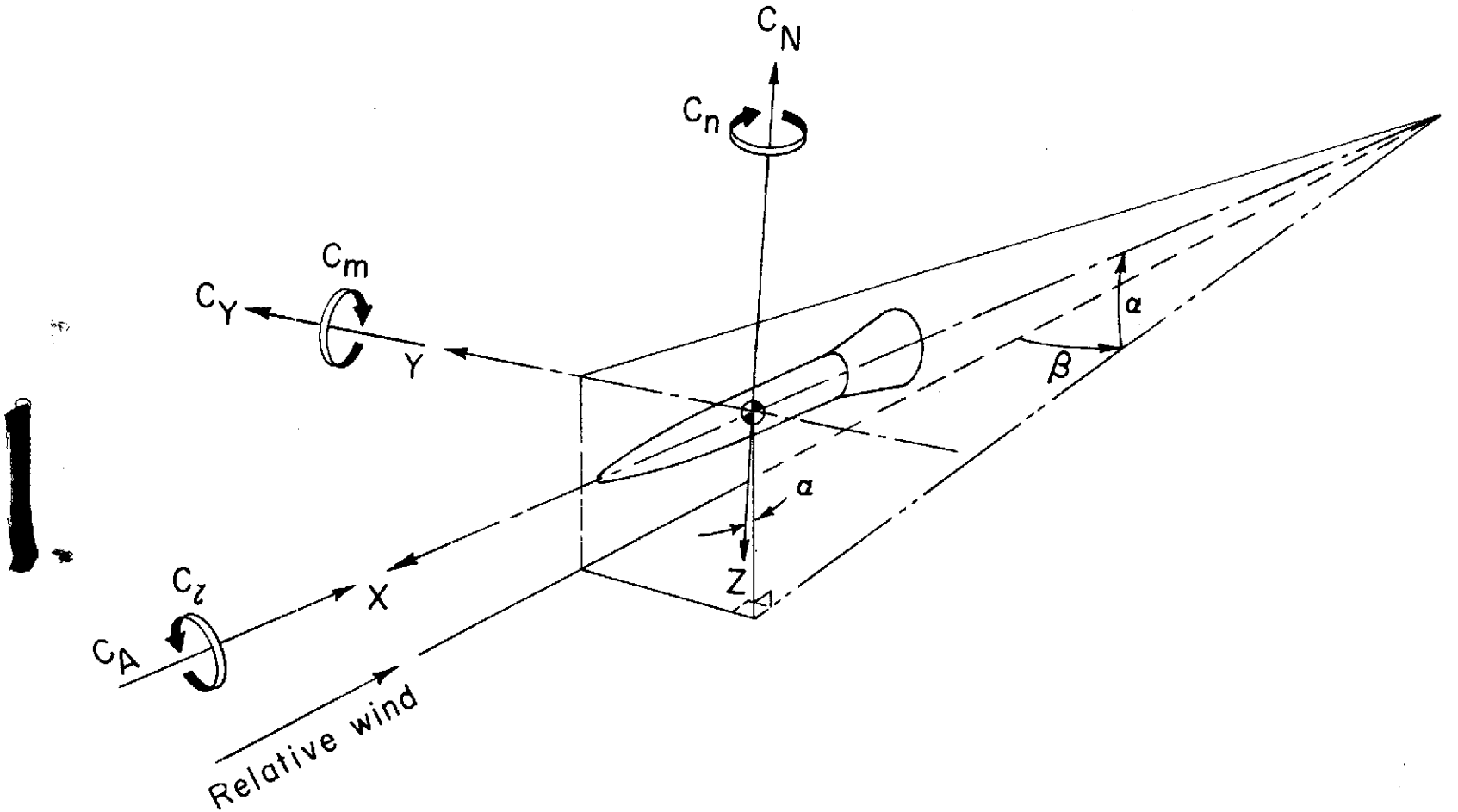

(a) Body axes.

Figure 1.- Systems of axes. Arrows indicate directions of positive forces, moments, and angles.

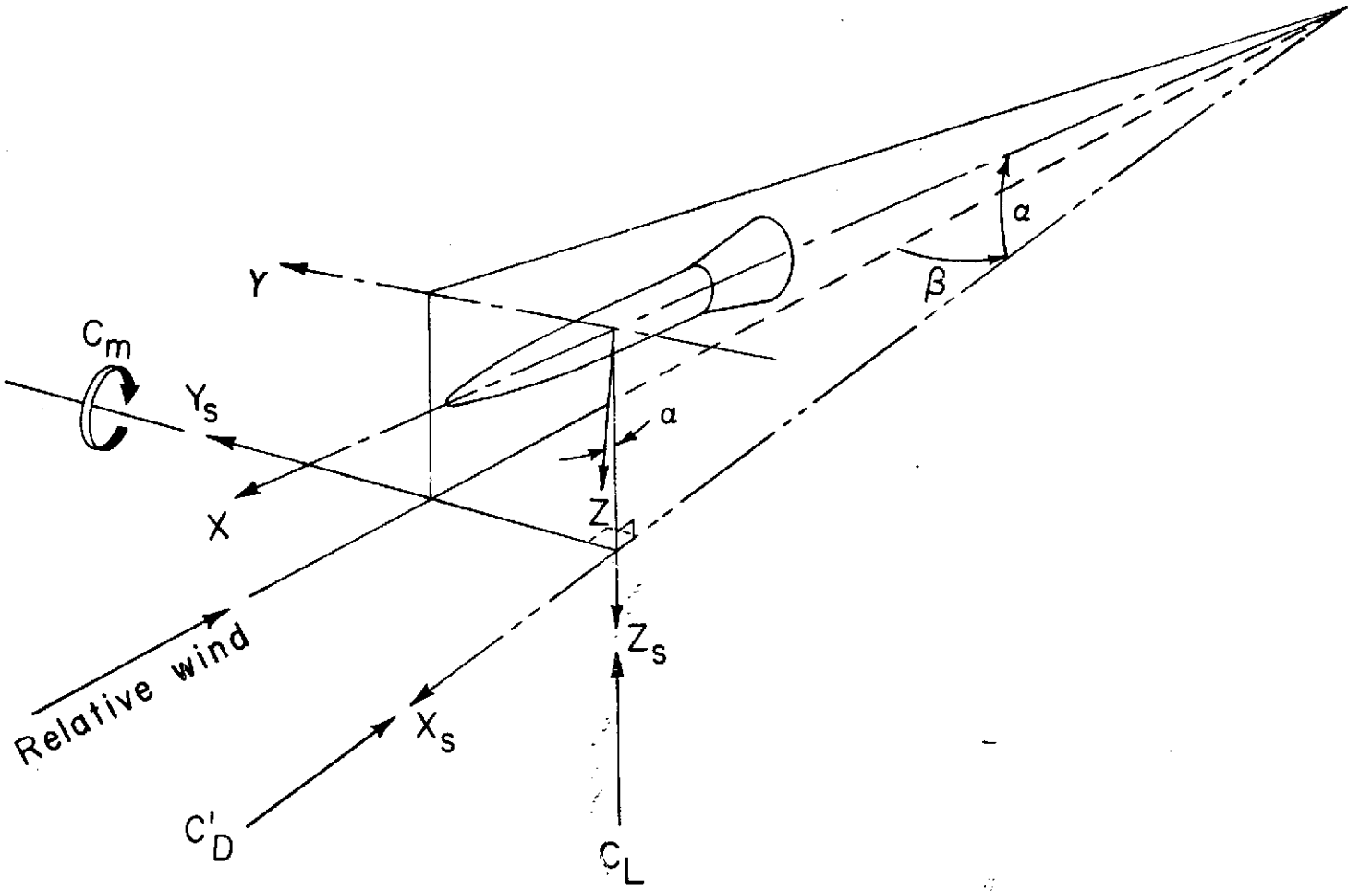

(b) Stability axes.

Figure 1.- Concluded.

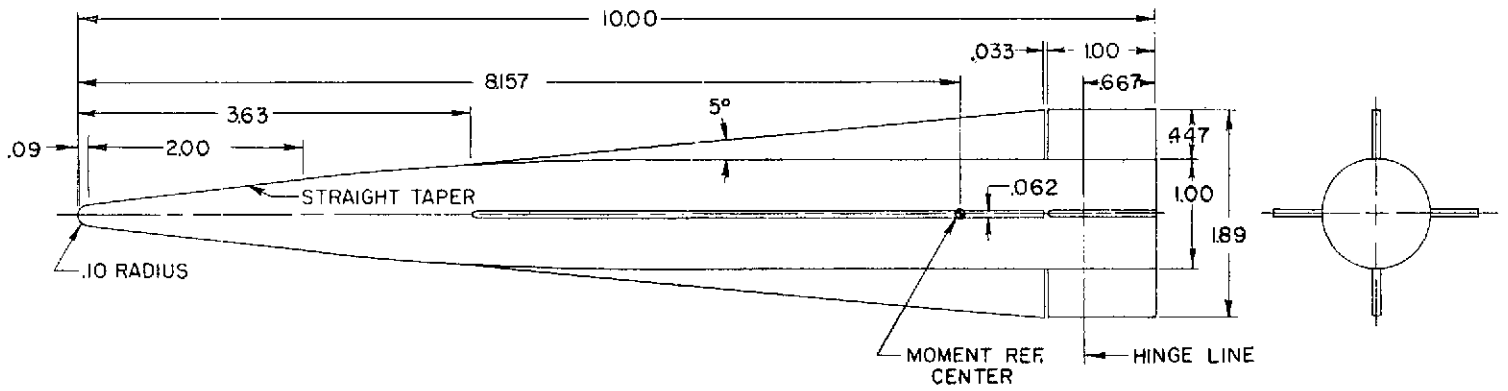

(a) Model with delta fins and trailing-edge controls.

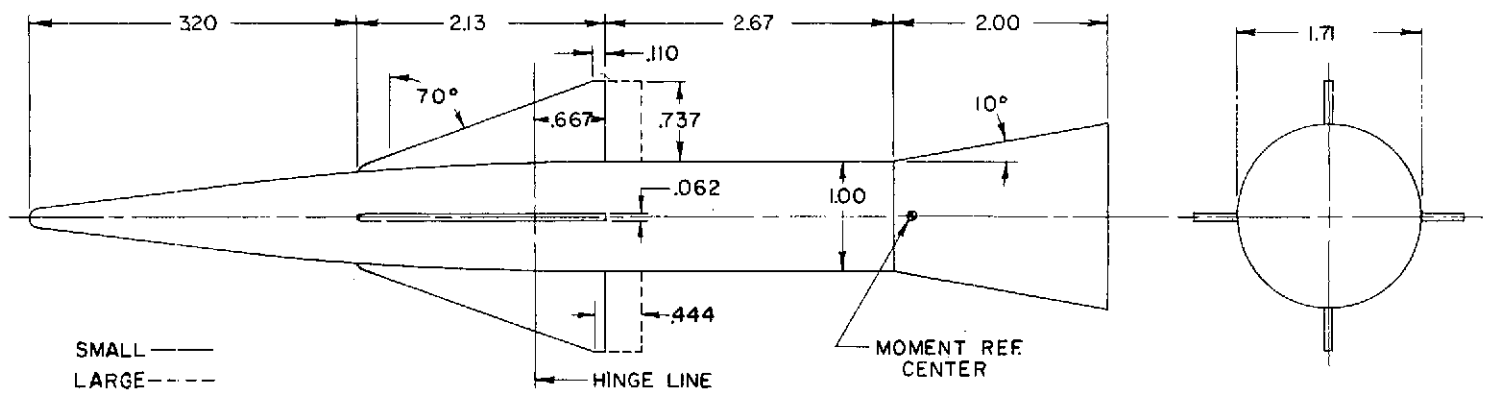

(b) Model with flared skirt and large and small canard controls.

Figure 2.- Missile configurations tested. All linear dimensions are in diameters.

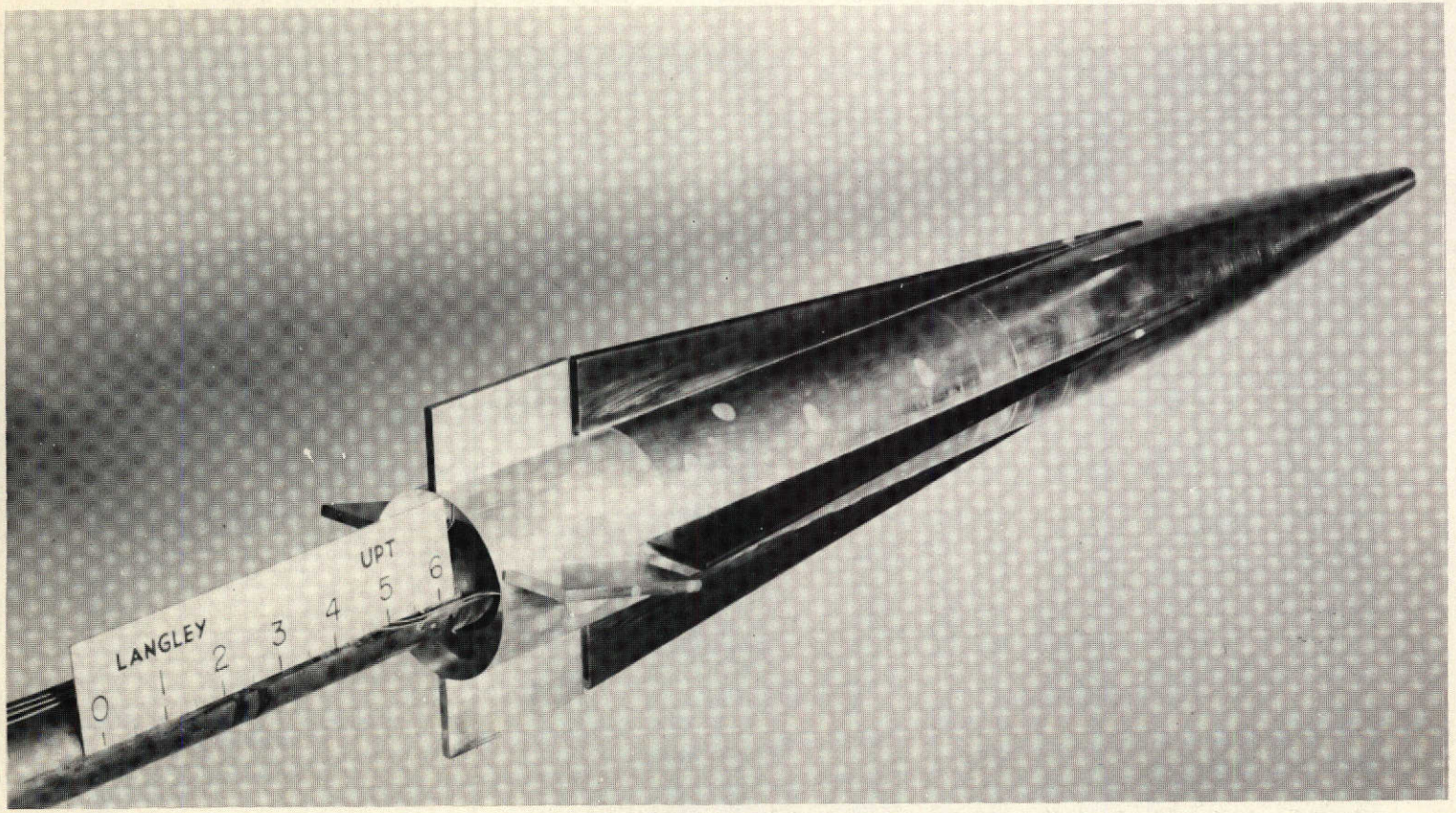

(a) Model with delta fins and trailing-edge controls. L-58-360

Figure 3.- Photographs of models.

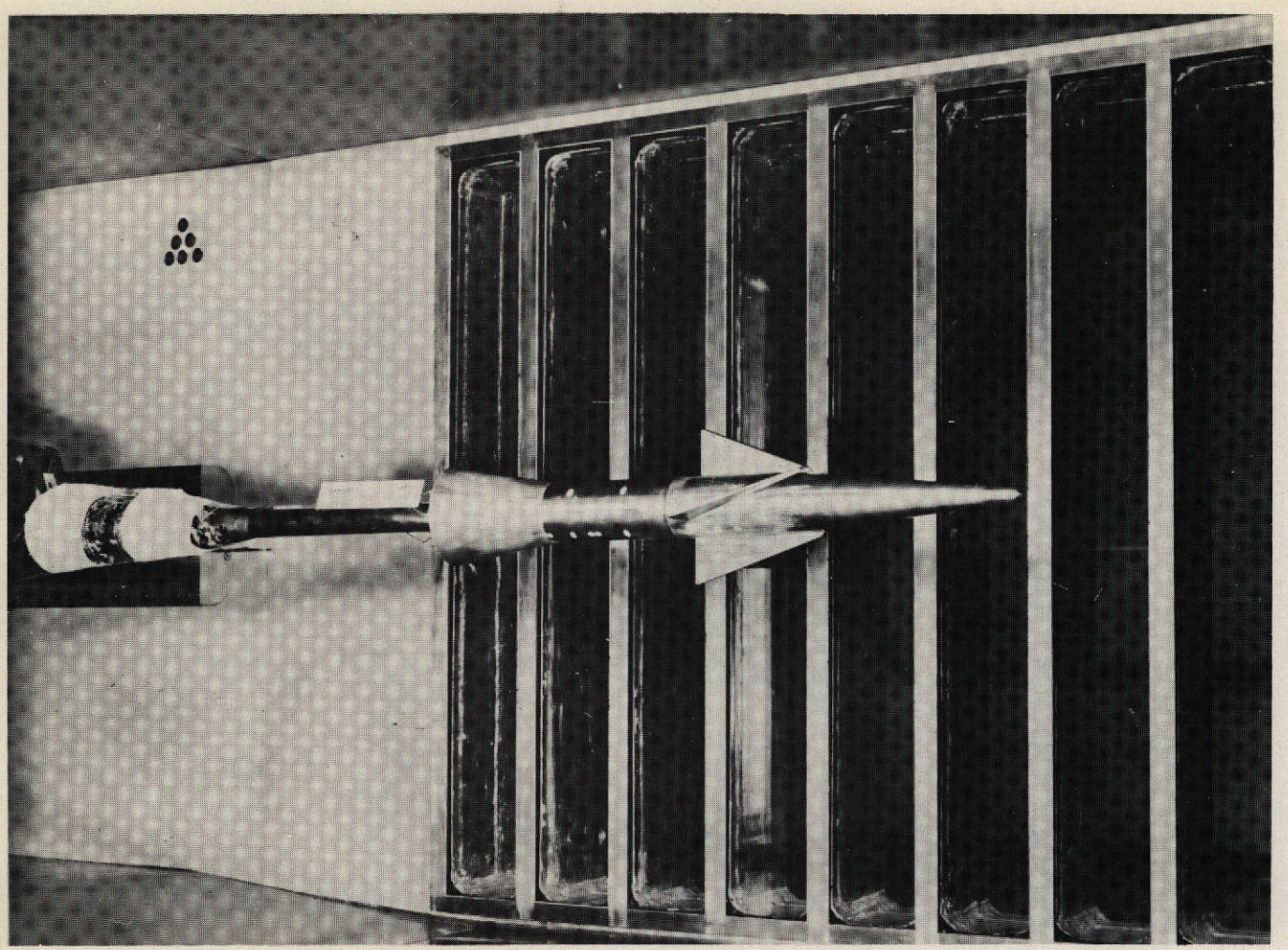

(b) Model with flared skirt and small canard controls. L-58-592

Figure 3.- Concluded.

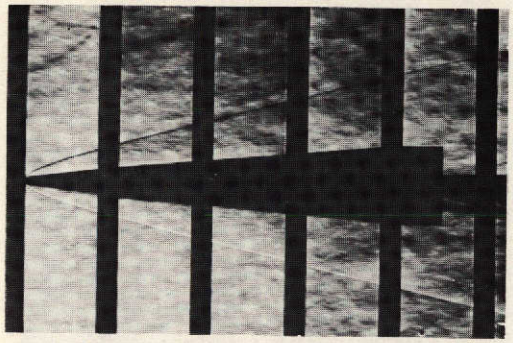

α = 0.9°

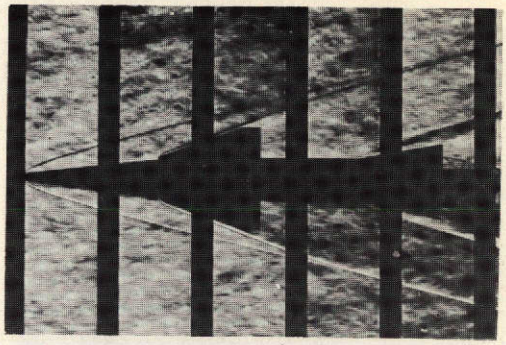

α = 0.9°

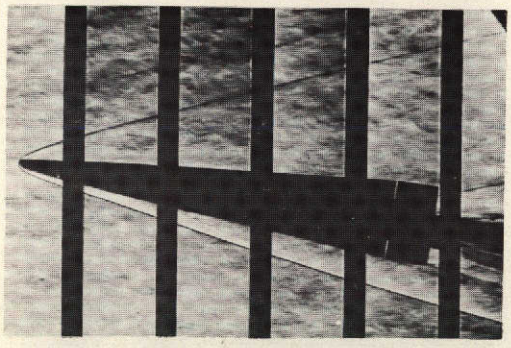

α = 9.0°

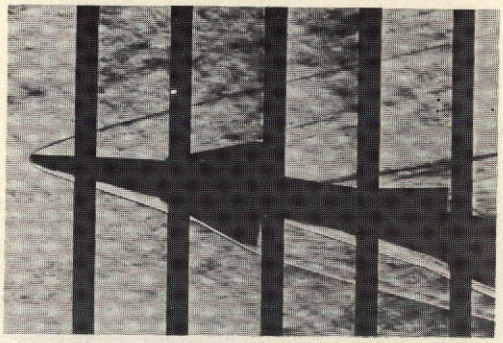

α = 9.1°

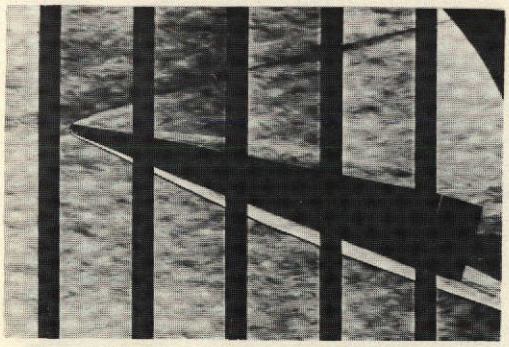

α = 17.2°

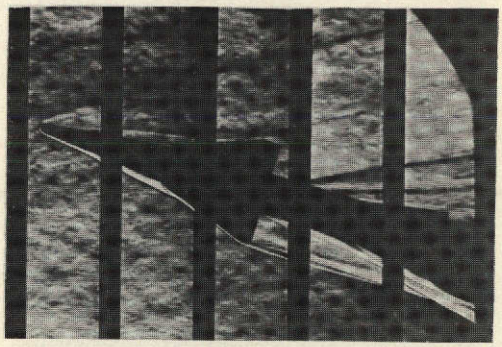

α = 17.3°

L-59-6041

(a) Model with delta fins and trailing-edge controls.

(b) Model with flared skirt and large canard controls.

Figure 4.- Typical schlieren photographs. $\beta = 0^{\circ}$.

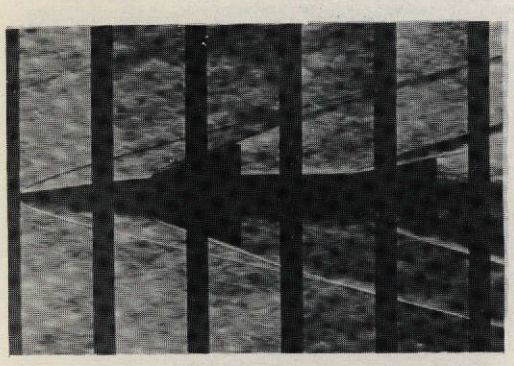

α = 0.9°

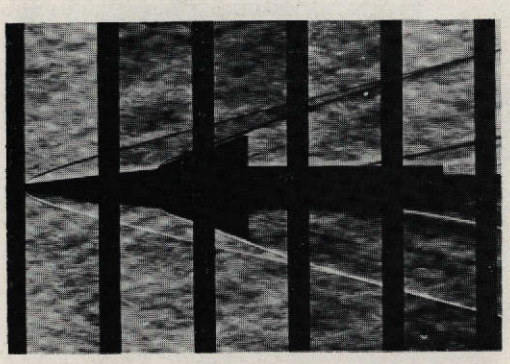

α = 0.9°

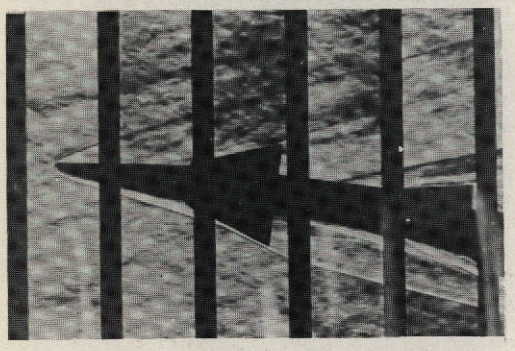

α = 9.1°

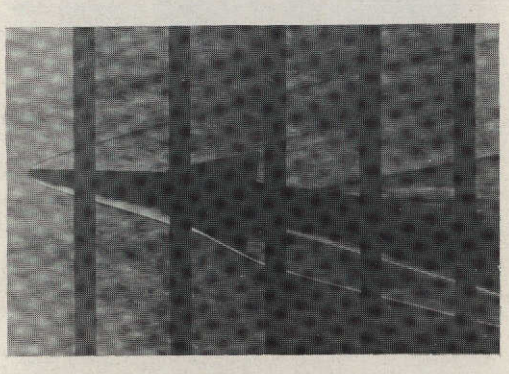

α = 9.1°

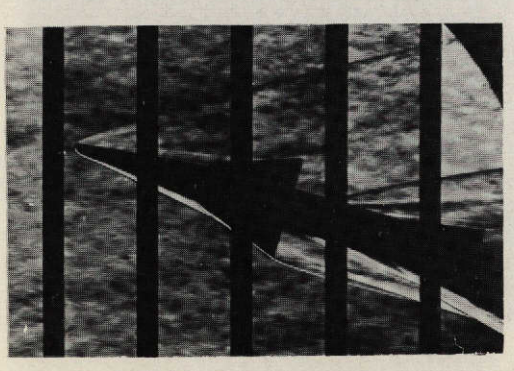

α = 17.3°

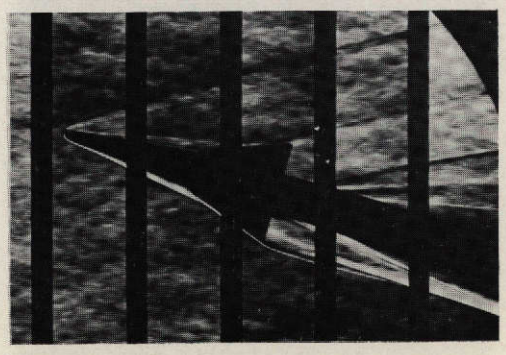

α = 17.3°

L-59-6042

(c) Model with flared skirt and small canard controls.

(d) Model with small canard controls.

Figure 4.- Concluded.

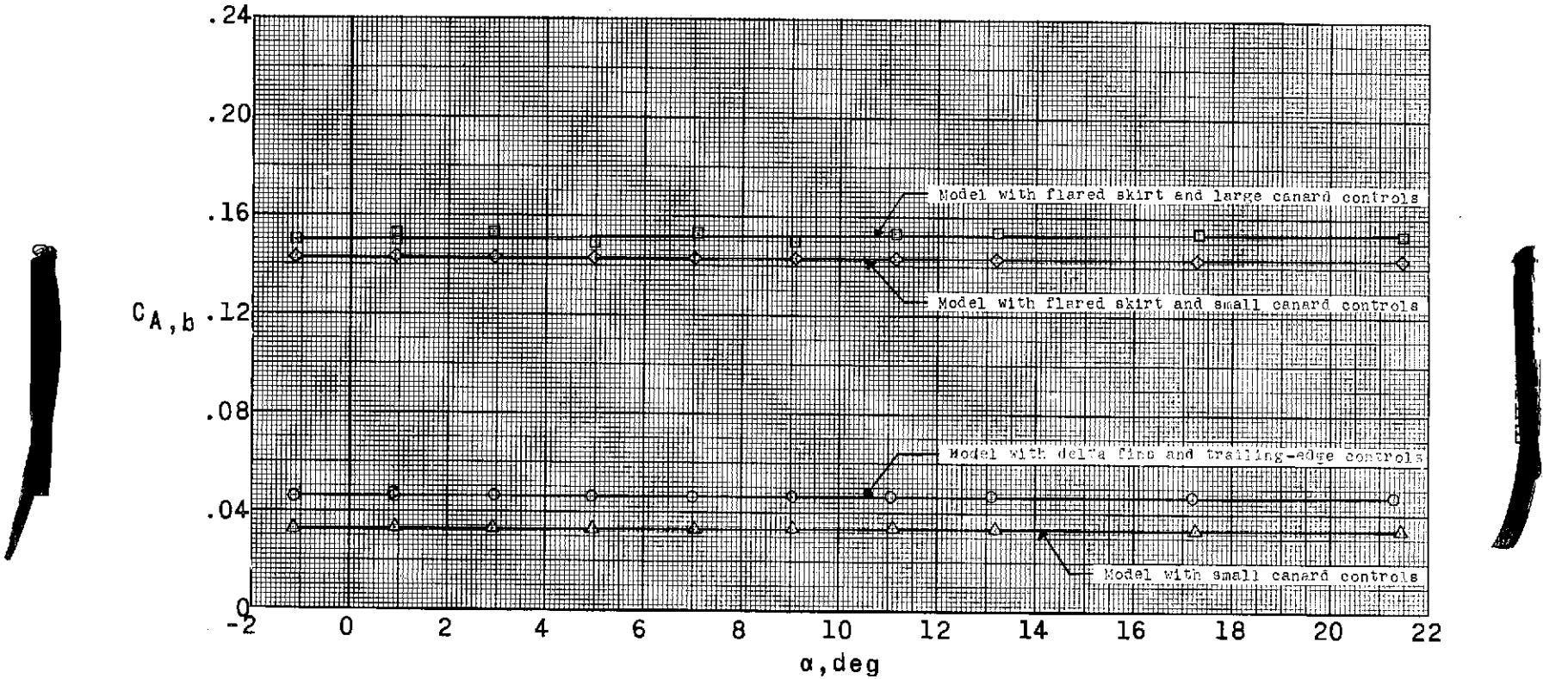

Figure 5.- Variation of typical base axial-force coefficients with angle of attack. $\beta = 0^{\circ}$.

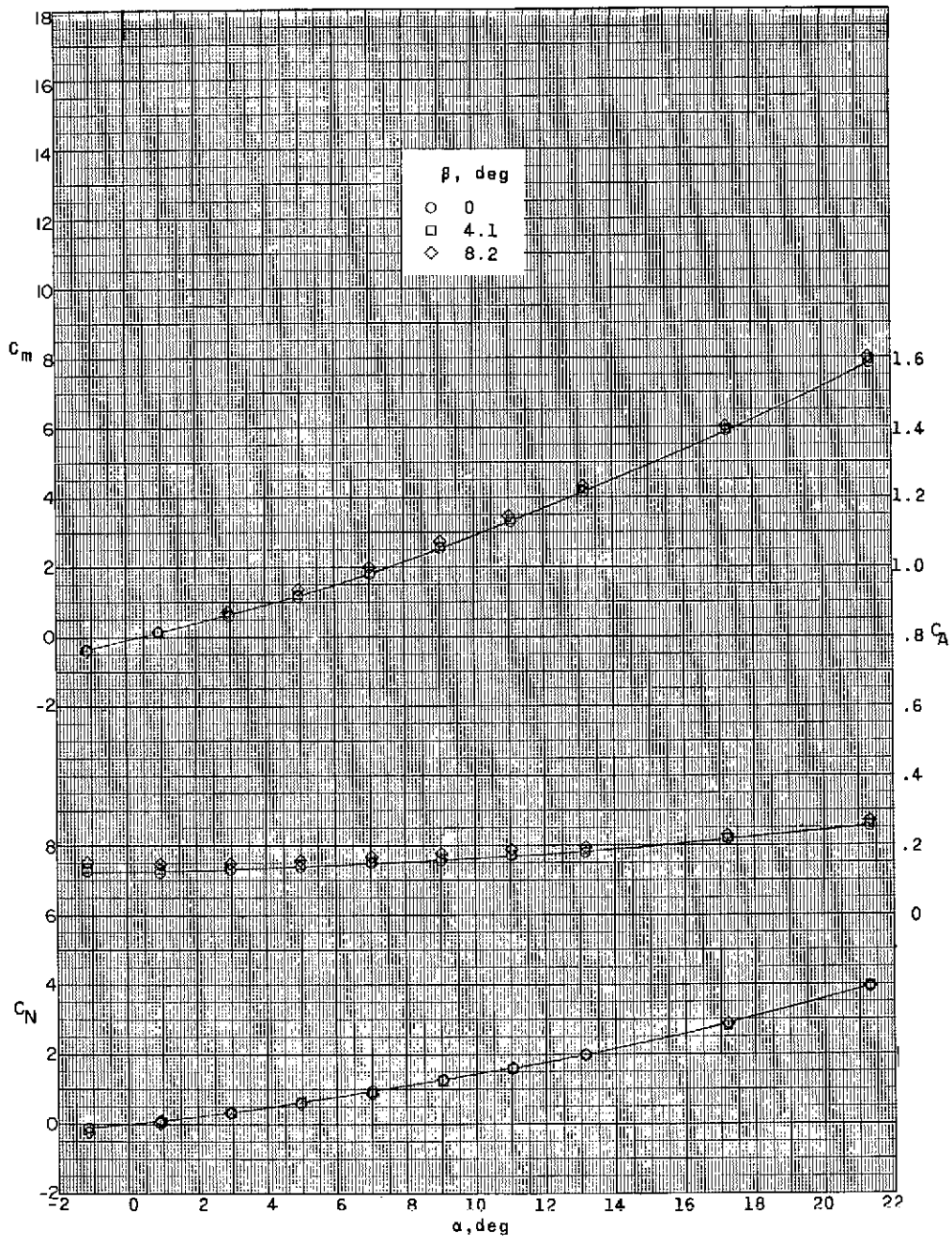

(a) $\delta_e = 0^\circ$; $\delta_r = \delta_a = 0^\circ$.

Figure 6.- Effect of pitch, yaw, and differential control deflections on aerodynamic characteristics of model with delta fins and trailing-edge controls.

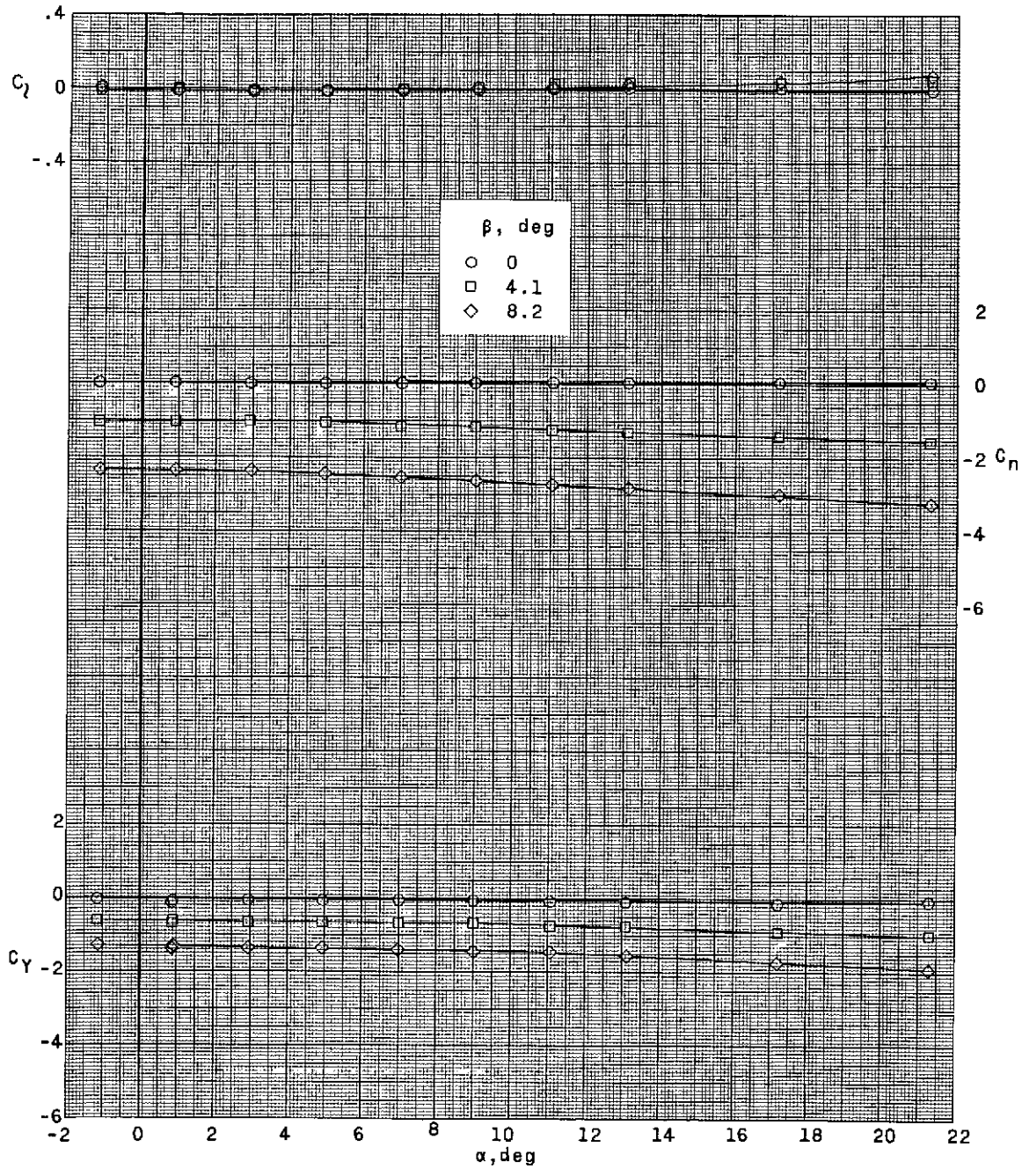

(a) $\delta_e = 0^\circ$; $\delta_r = \delta_a = 0^\circ$. Concluded.

Figure 6.- Continued.

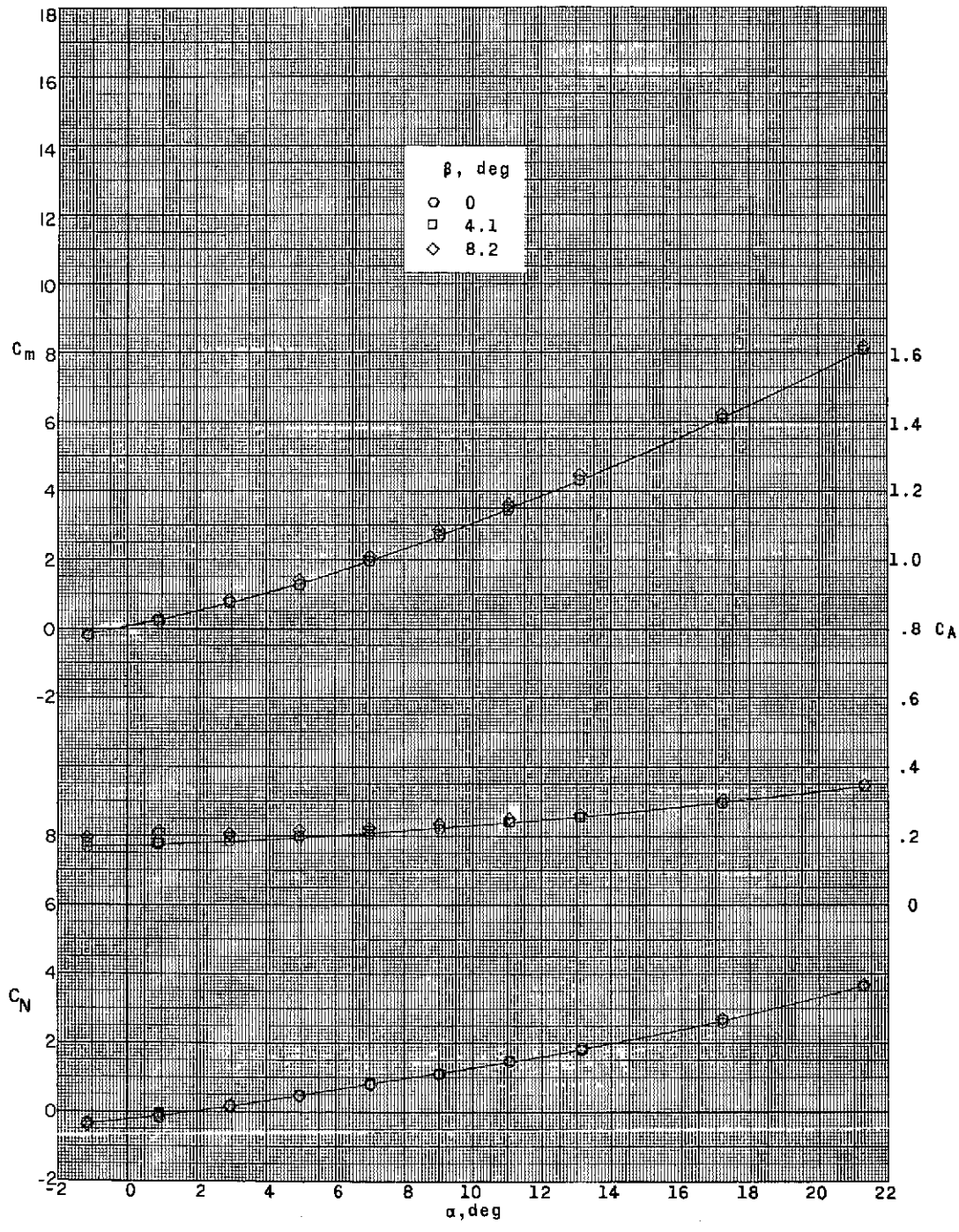

(b) $\delta_e = -10.0^\circ$; $\delta_r = \delta_a = 0^\circ$.

Figure 6.- Continued.

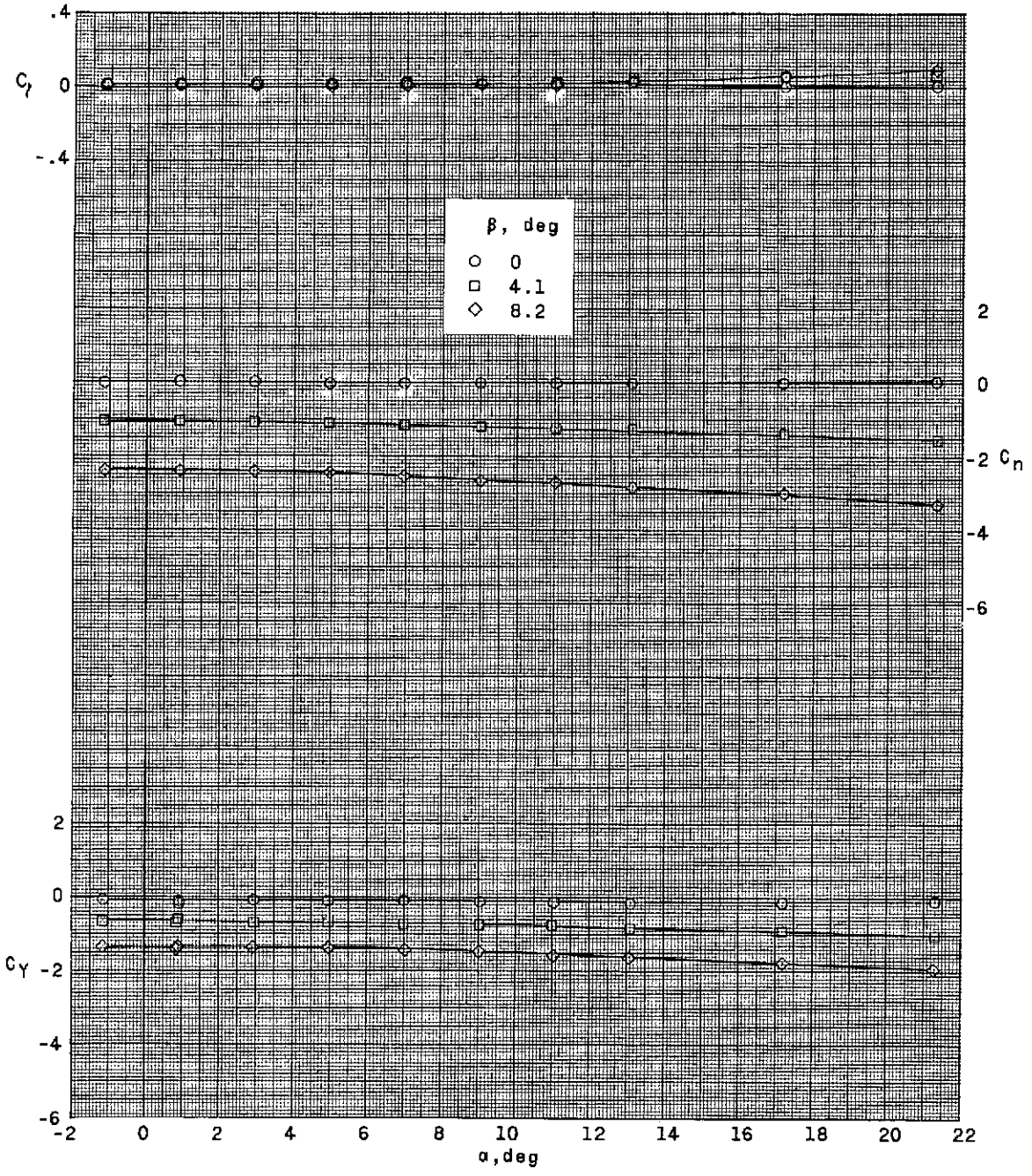

(b) $\delta_e = -10.0^o$; $\delta_r = \delta_a = 0^o$. Concluded.

Figure 6.- Continued.

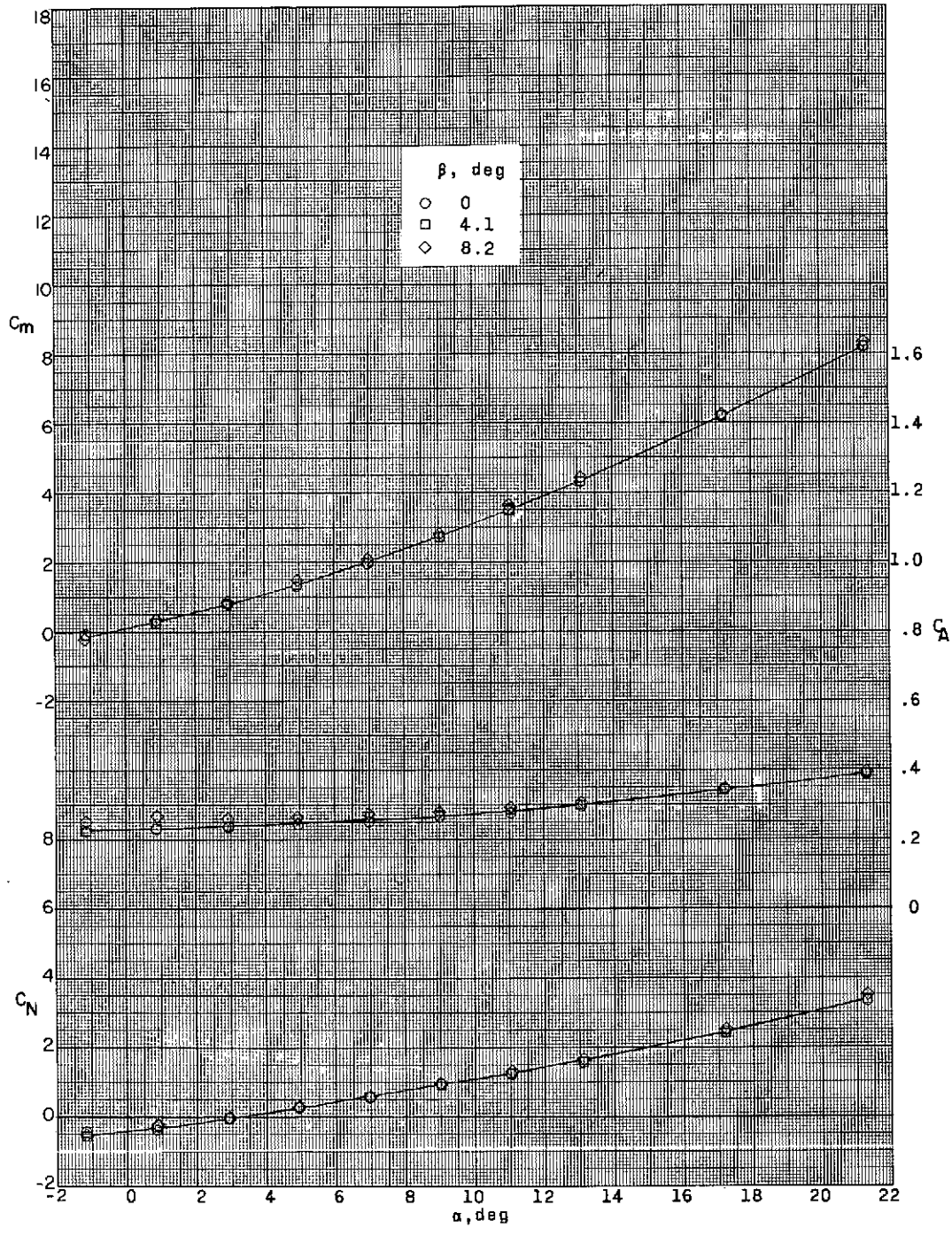

(c) $\delta_e = -15.1^\circ$; $\delta_r = \delta_a = 0^\circ$.

Figure 6.- Continued.

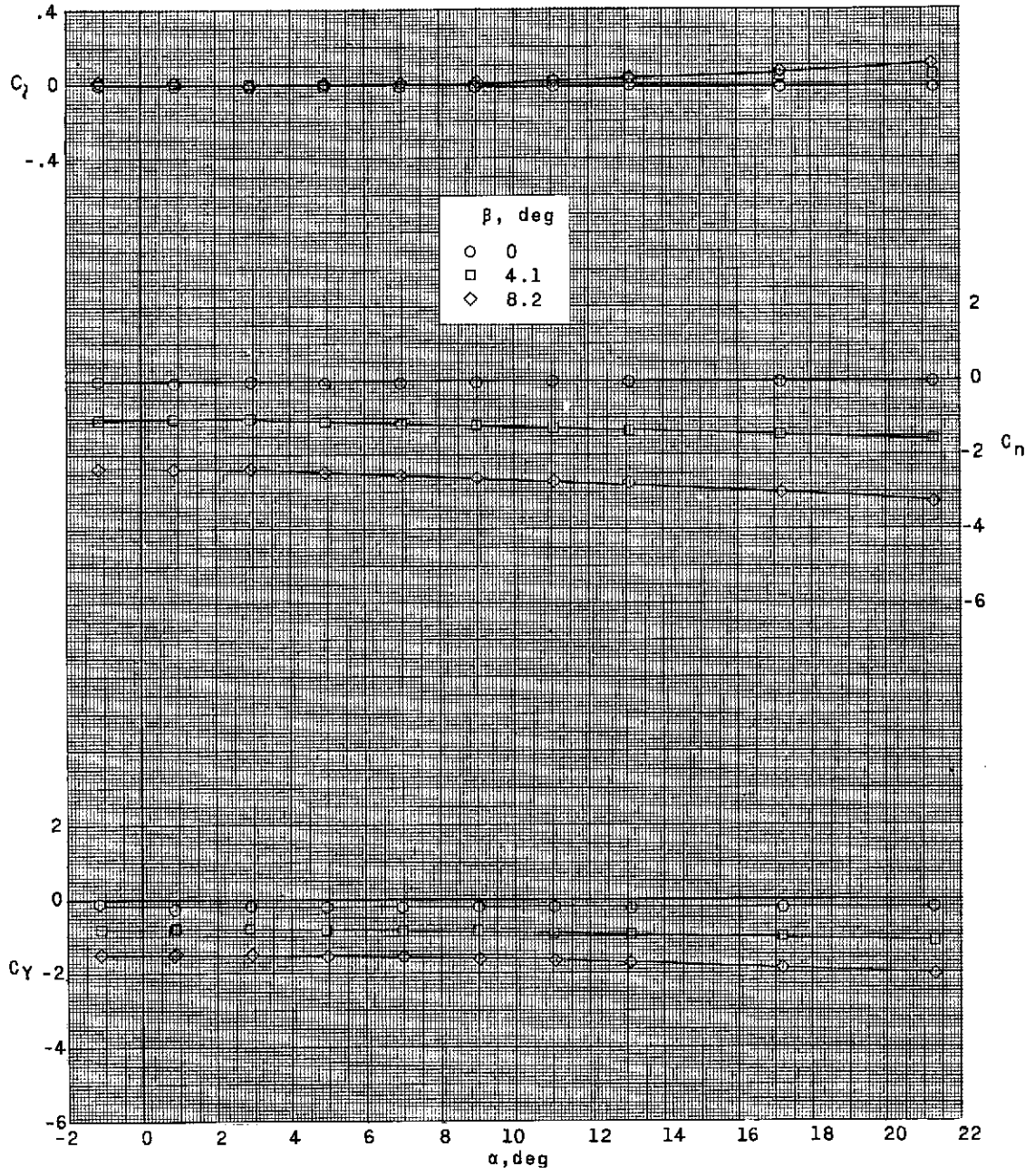

(c) $\delta_e = -15.1^\circ$; $\delta_r = \delta_a = 0^\circ$. Concluded.

Figure 6.- Continued.

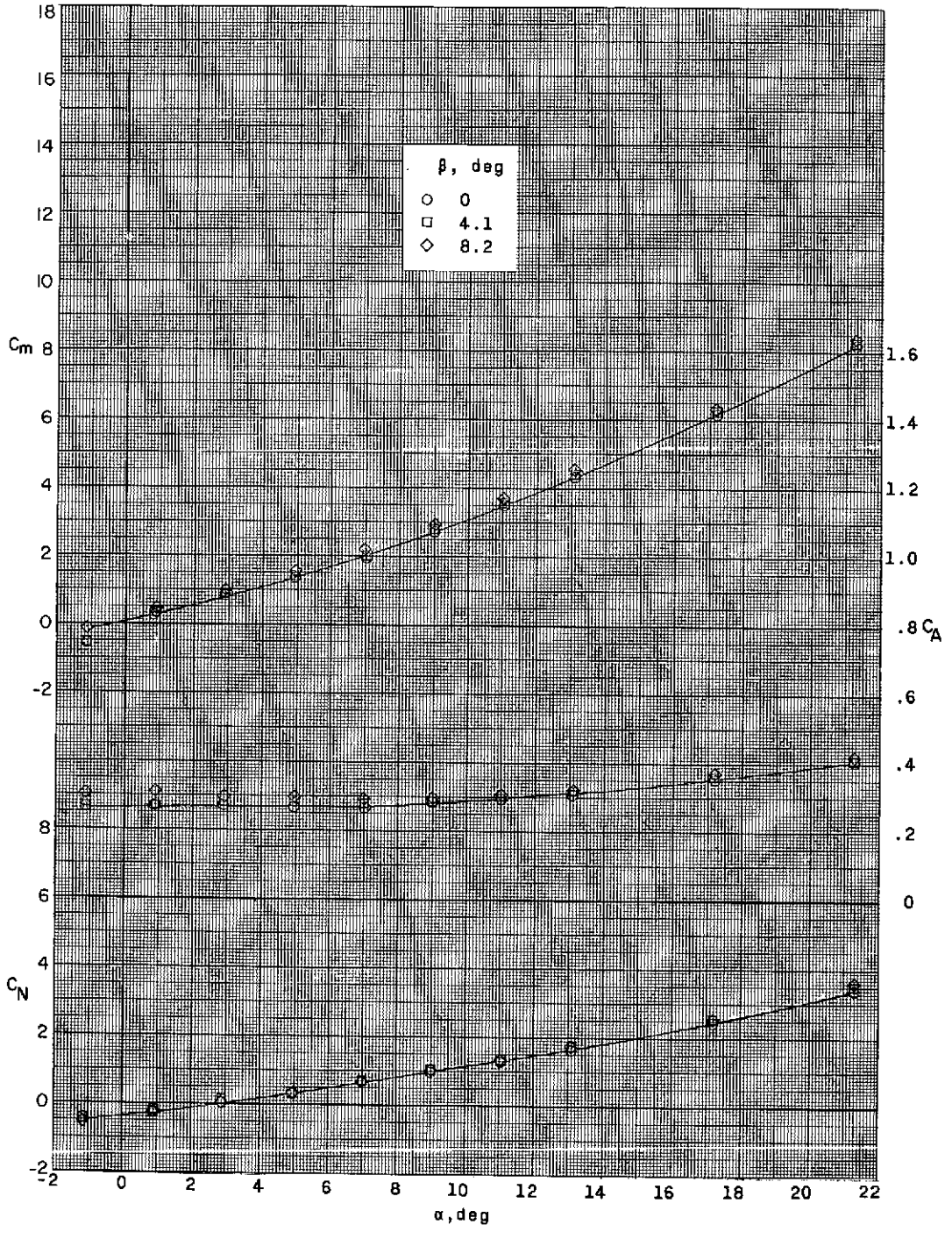

(d) $\delta_e = -20.0^\circ$; $\delta_r = \delta_a = 0^\circ$.

Figure 6.- Continued.

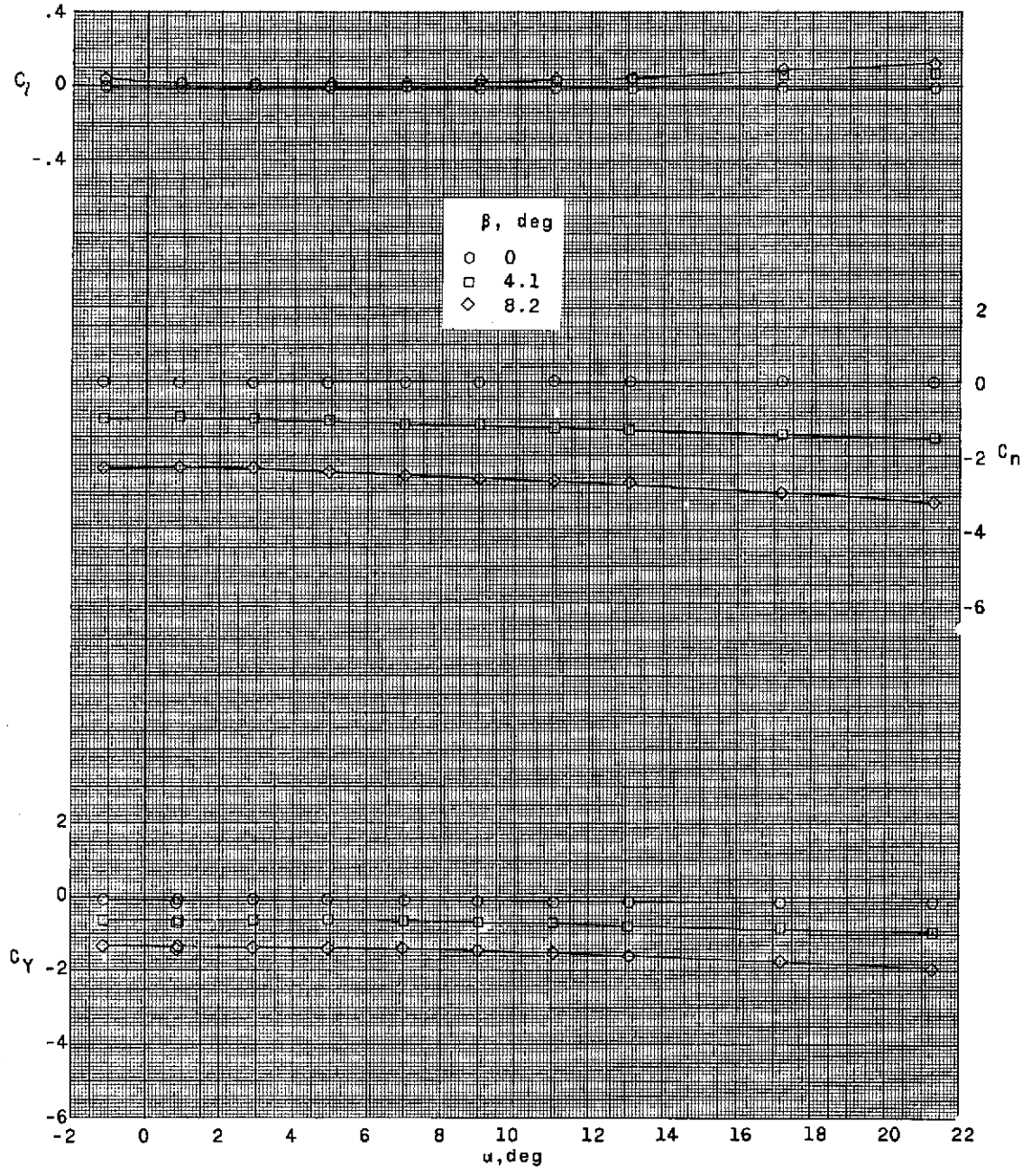

(d) $\delta_e = -20.0^\circ$; $\delta_r = \delta_a = 0^\circ$. Concluded.

Figure 6.- Continued.

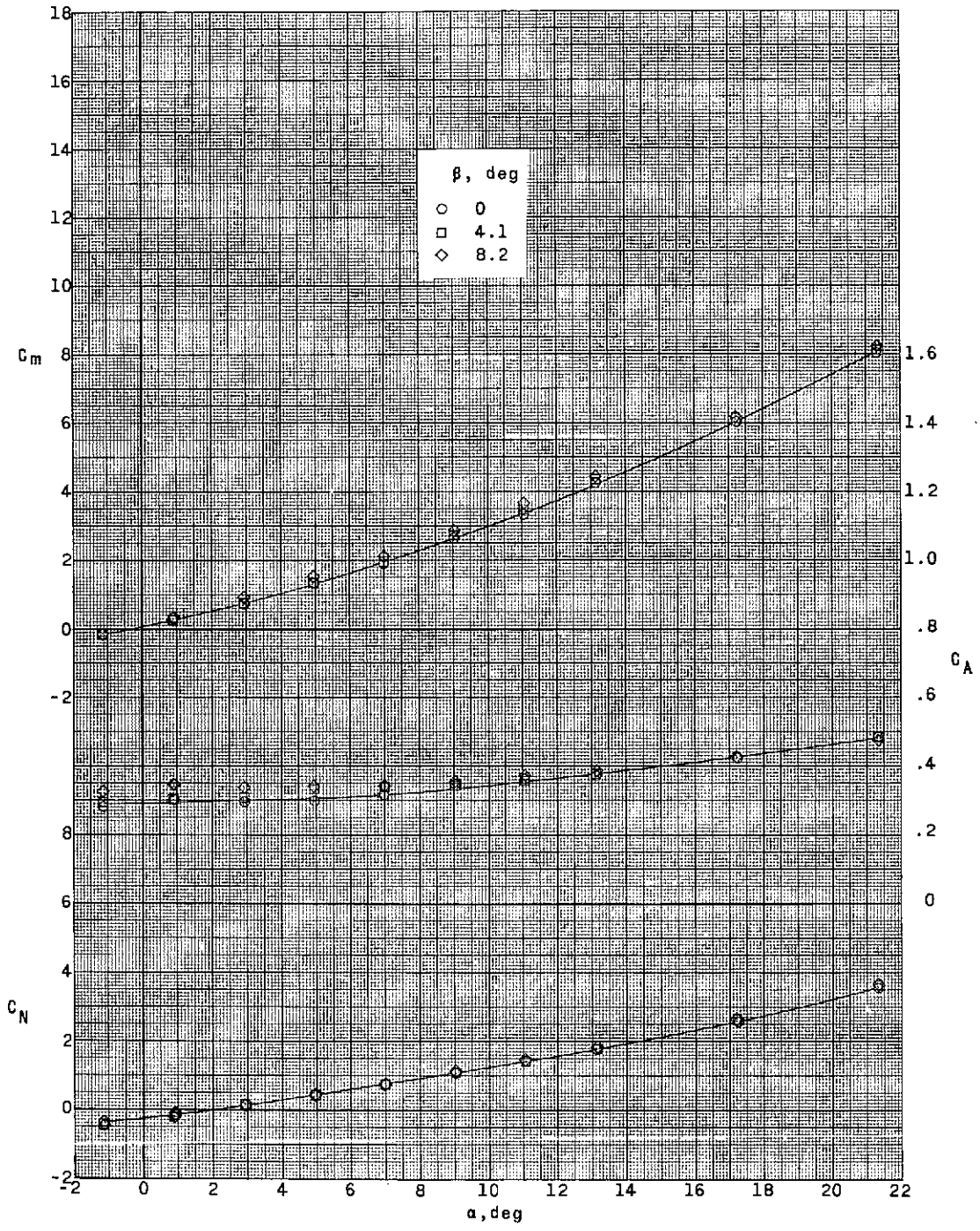

(e) $\delta_e = -15.0^\circ$; $\delta_r = 15.0^\circ$; $\delta_a = 0^\circ$.

Figure 6.- Continued.

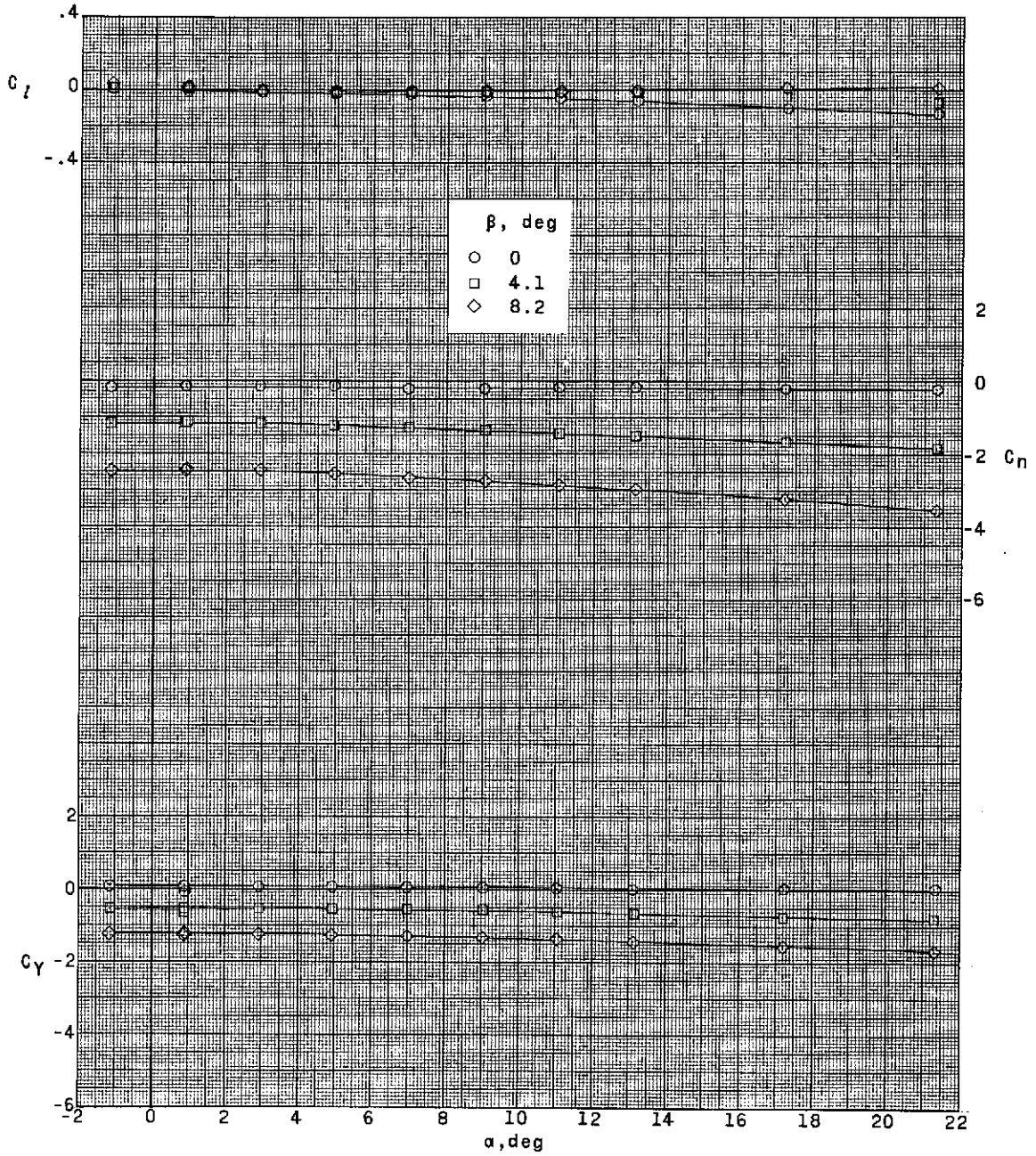

(e) $\delta_e = -15.0^\circ$; $\delta_r = 15.0^\circ$; $\delta_a = 0^\circ$. Concluded.

Figure 6.- Continued.

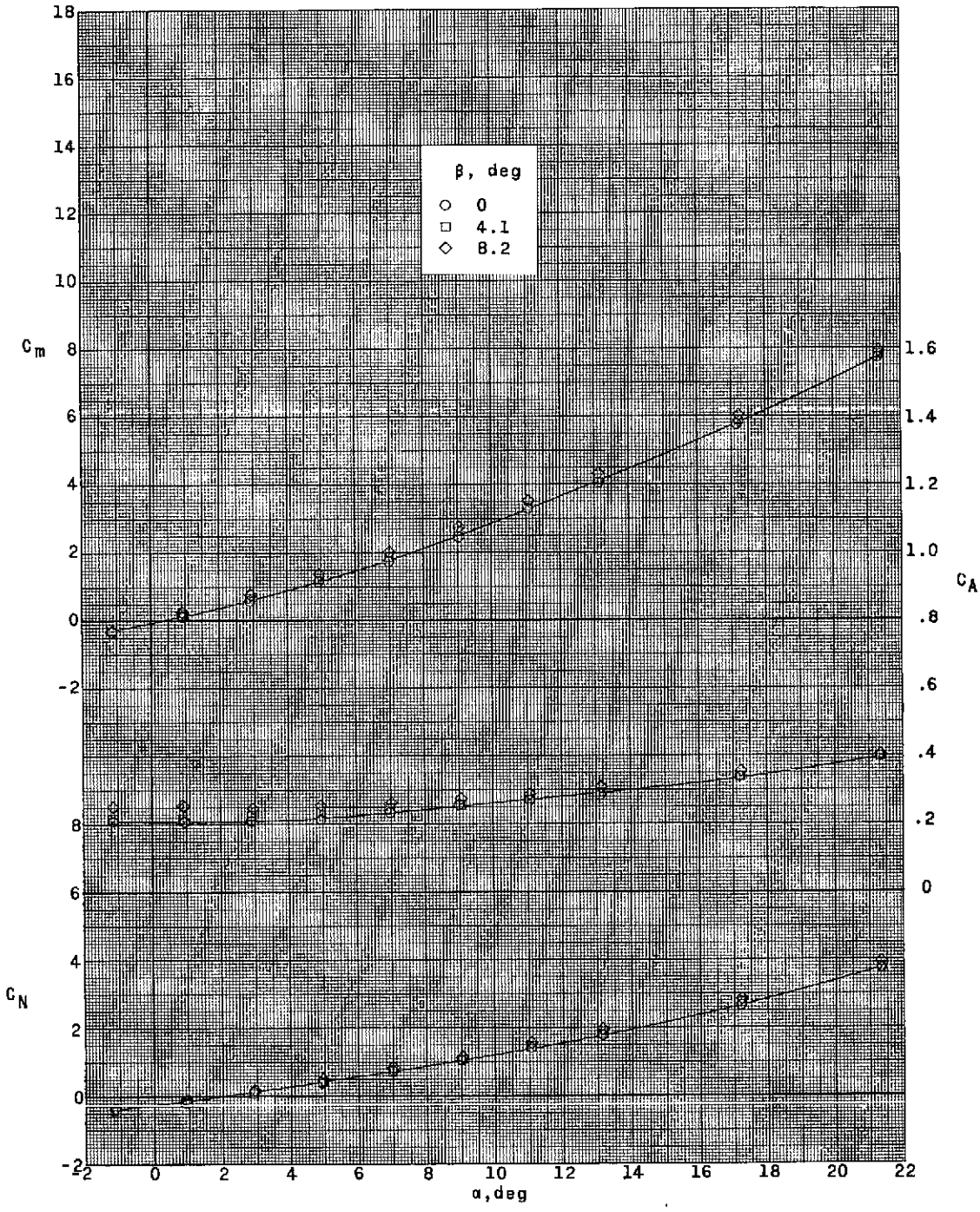

(f) $\delta_a = -40.0^\circ$; $\delta_e = \delta_r = 0^\circ$.

Figure 6.- Continued.

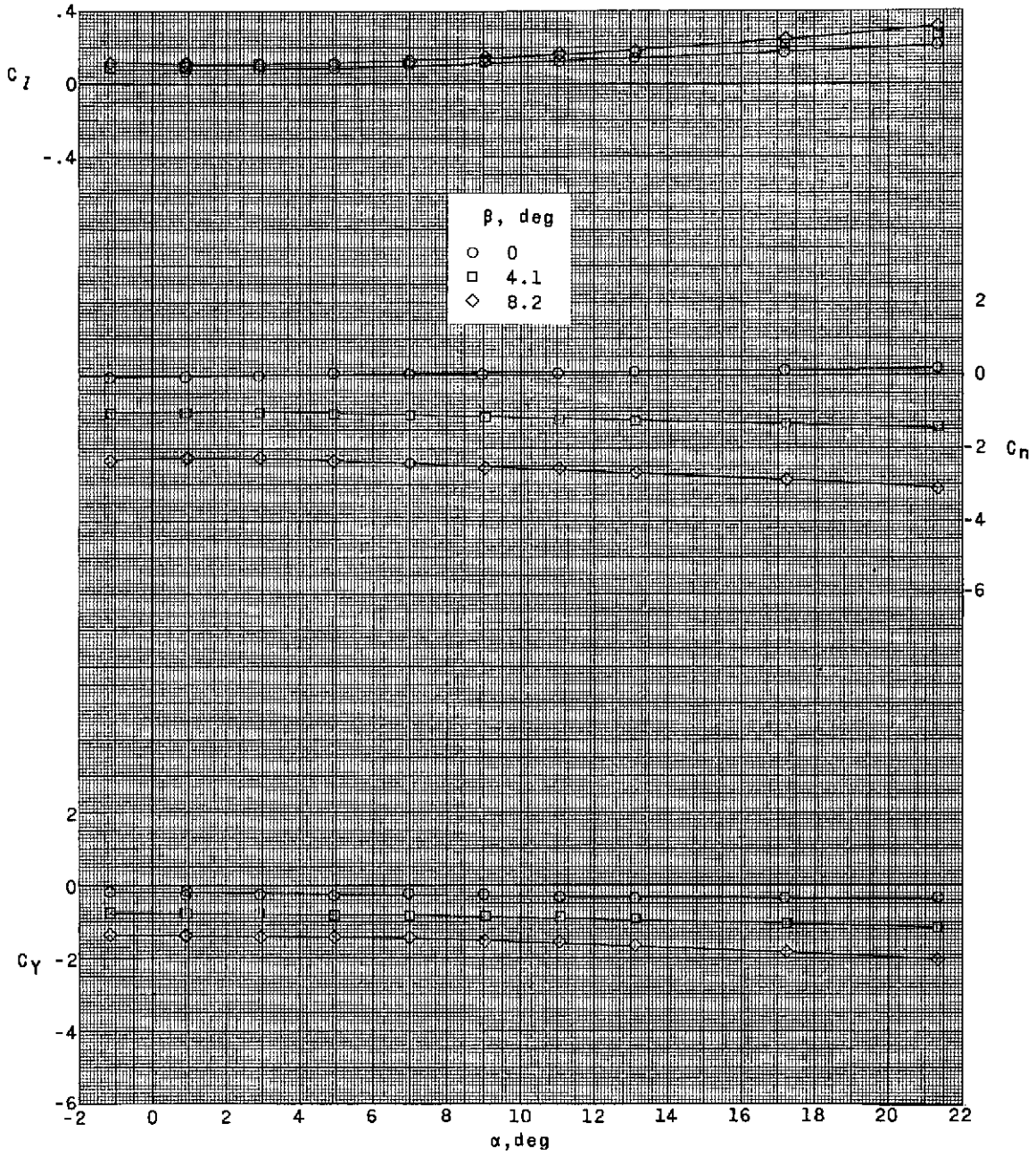

(f) $\delta_a = -40.0^\circ$; $\delta_e = \delta_r = 0^\circ$. Concluded.

Figure 6.- Concluded.

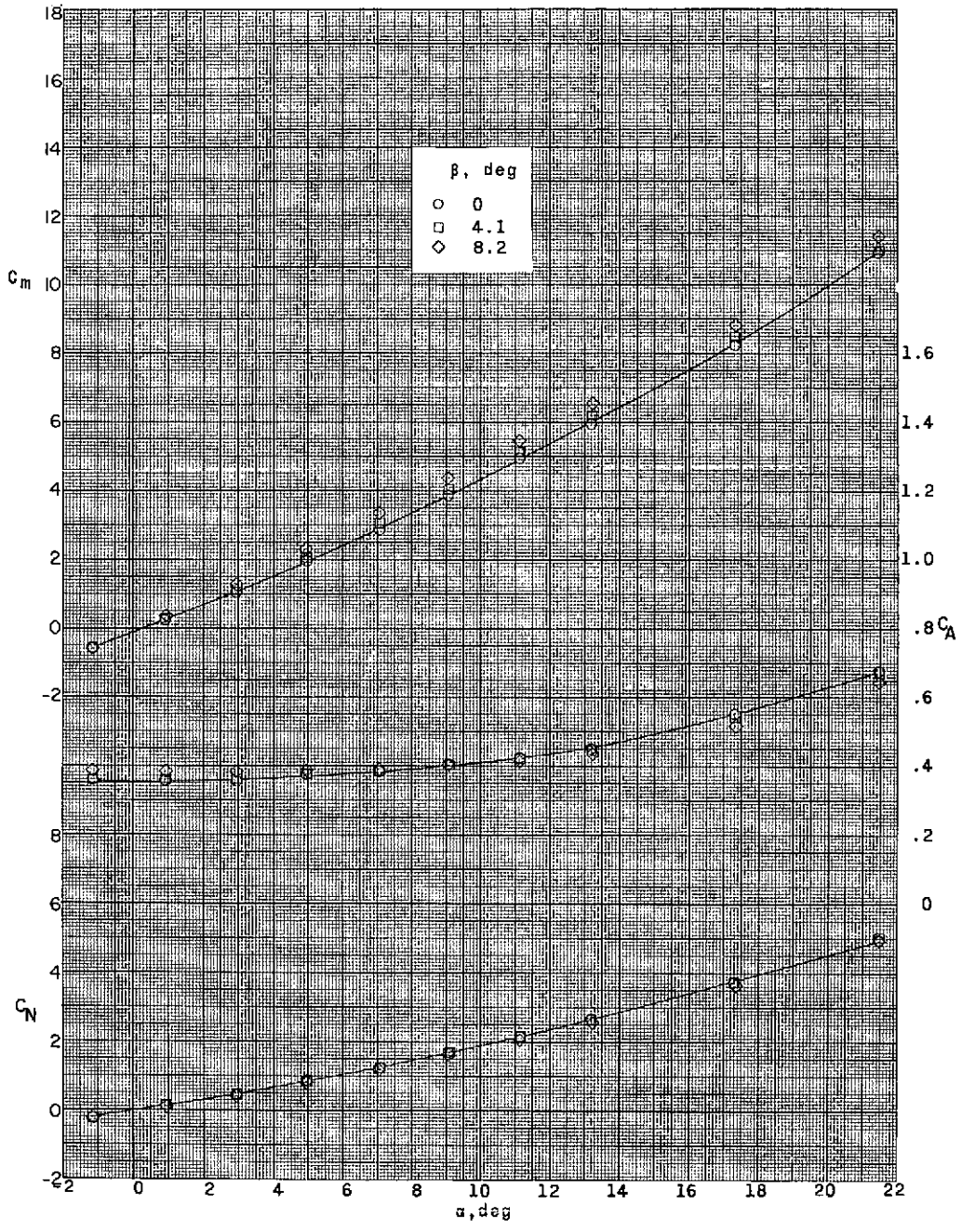

(a) $\delta_e = 0^\circ$; $\delta_r = \delta_a = 0^\circ$.

Figure 7.- Effect of pitch-control deflection on aerodynamic characteristics of model with flared skirt and large canard controls.

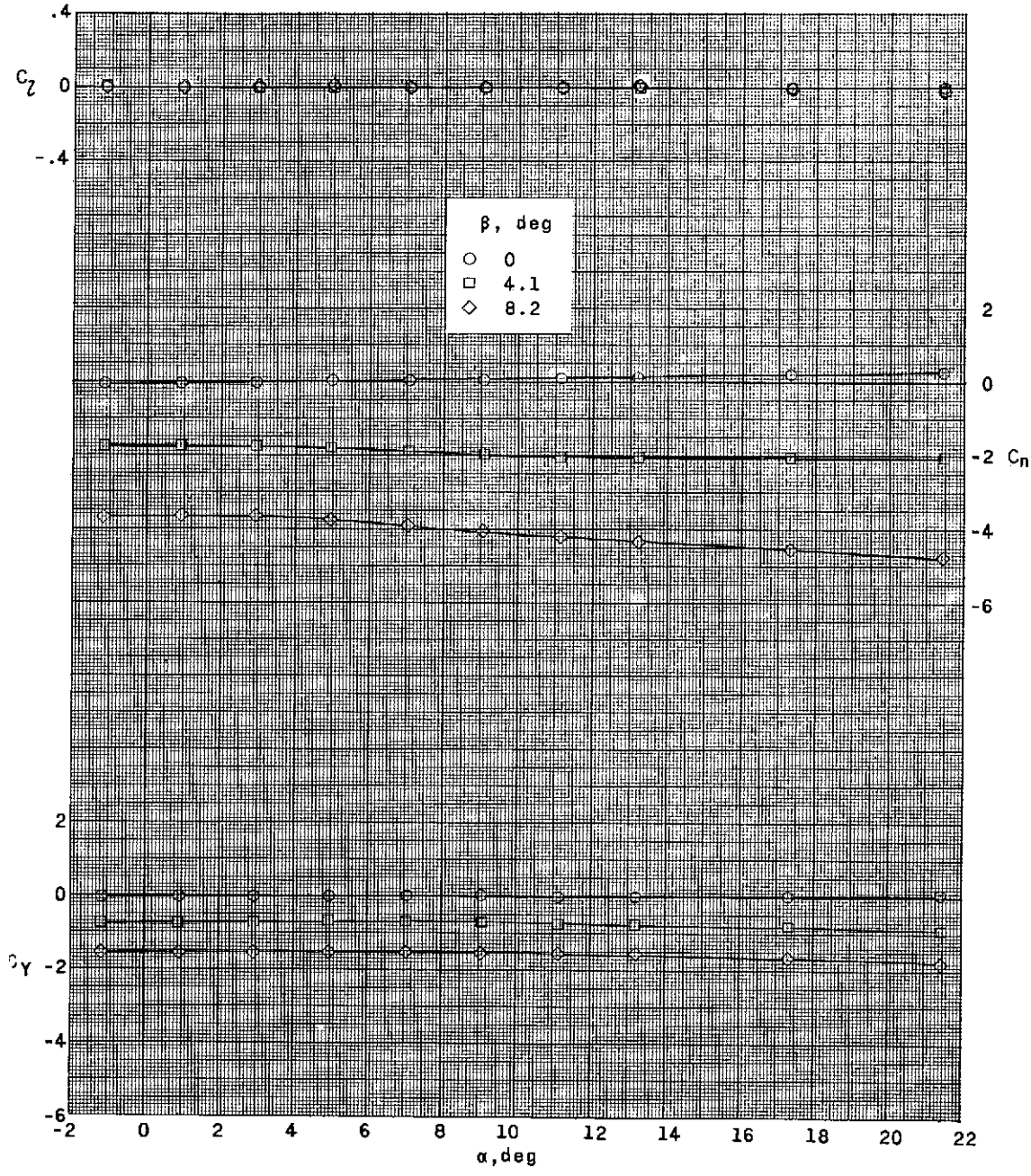

(a) $\delta_e = 0^o$; $\delta_r = \delta_a = 0^o$. Concluded.

Figure 7.- Continued.

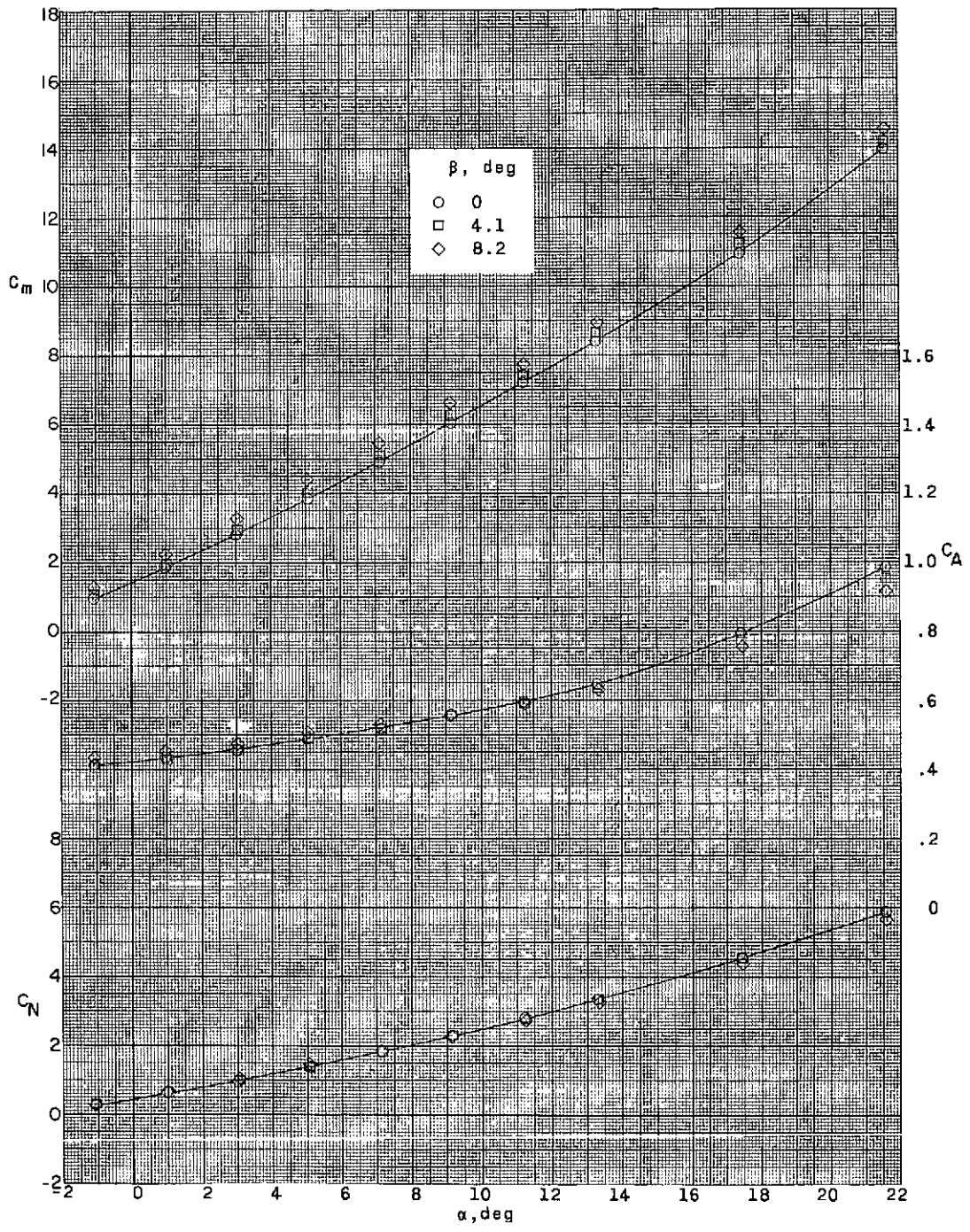

(b) $\delta_e = 10.0^\circ$; $\delta_r = \delta_a = 0^\circ$.

Figure 7.- Continued.

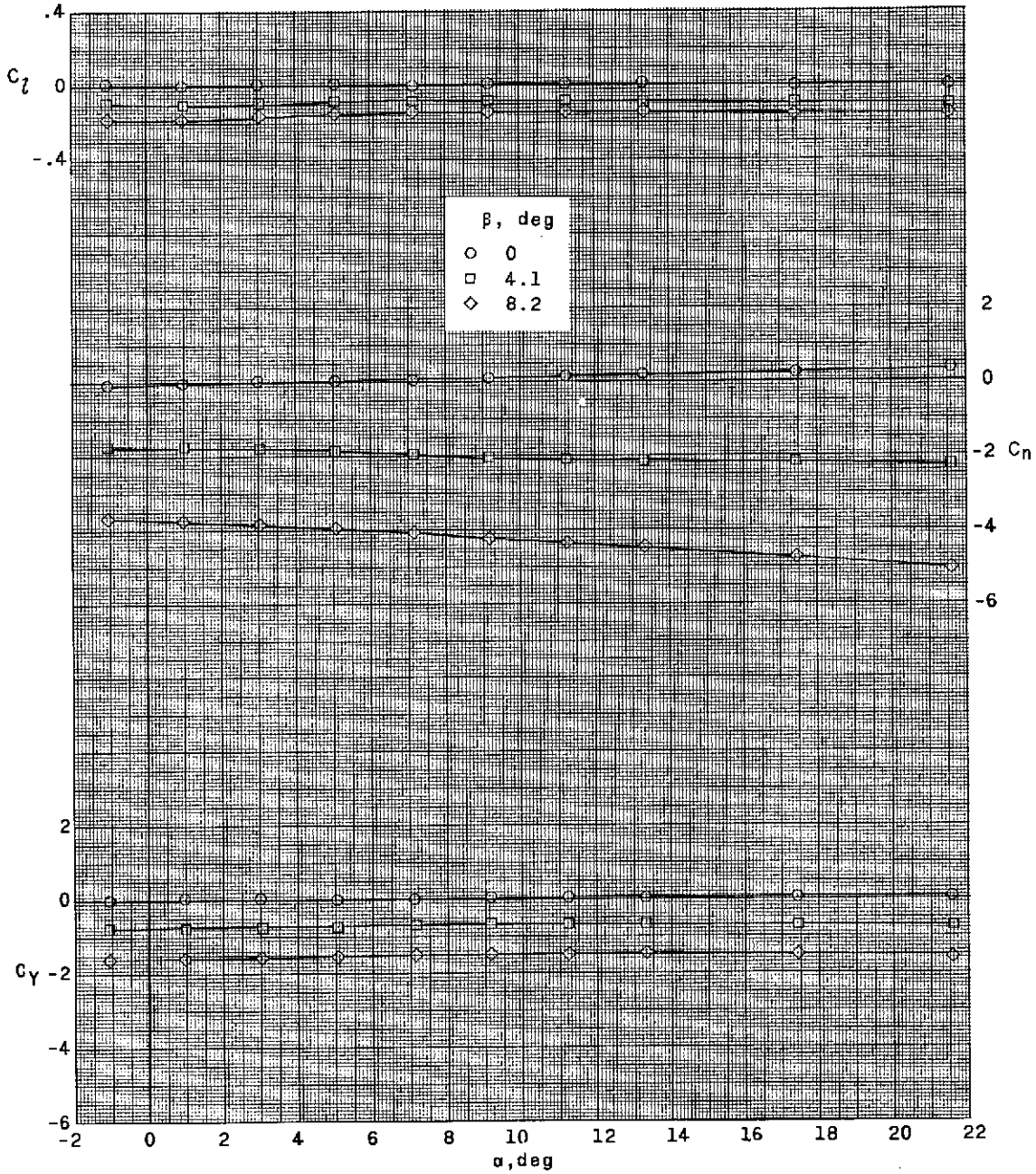

(b) $\delta_e = 10.0^\circ$; $\delta_r = \delta_a = 0^\circ$. Concluded.

Figure 7.- Continued.

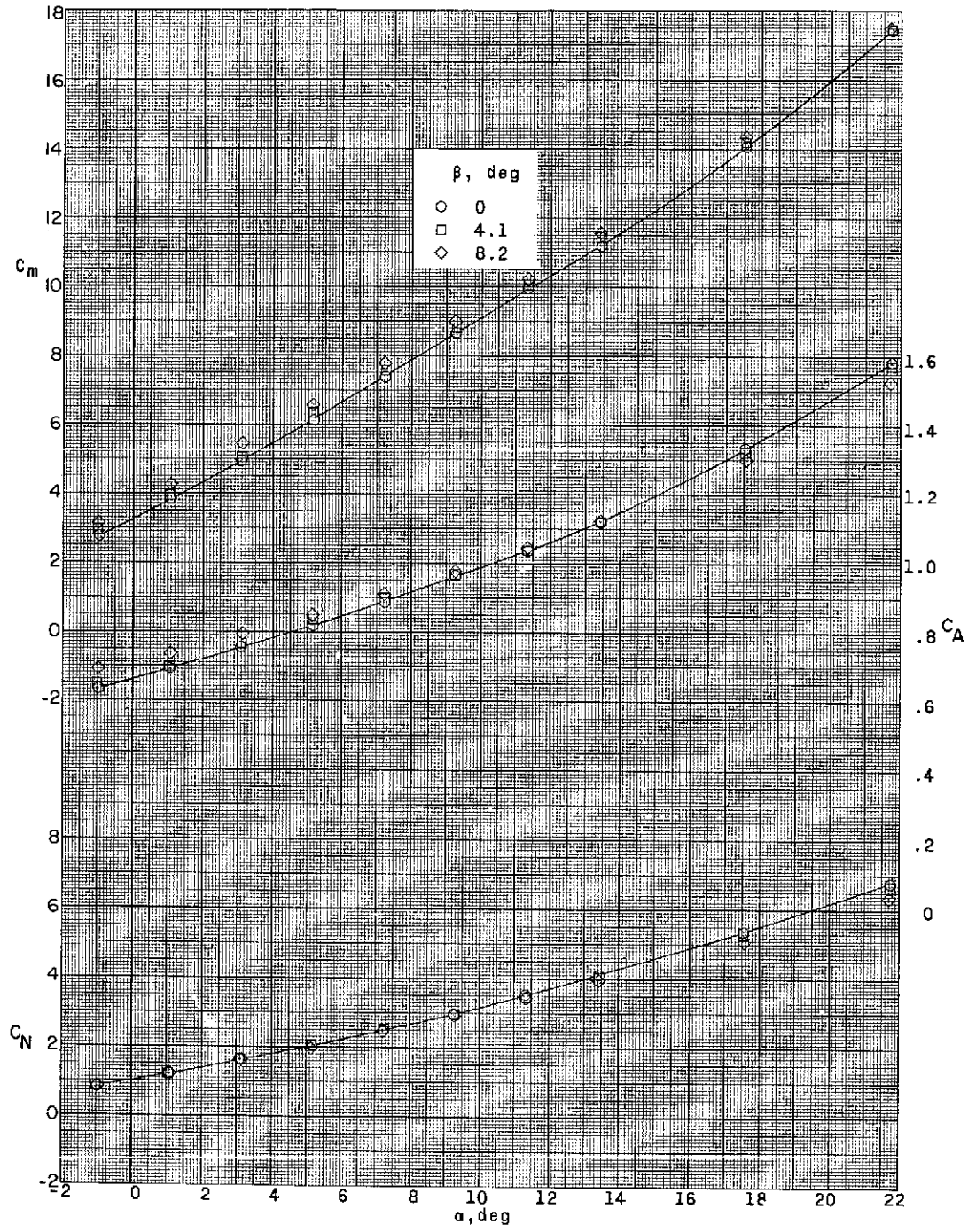

(c) $\delta_e = 20.0^\circ$; $\delta_r = \delta_a = 0^\circ$.

Figure 7.- Continued.

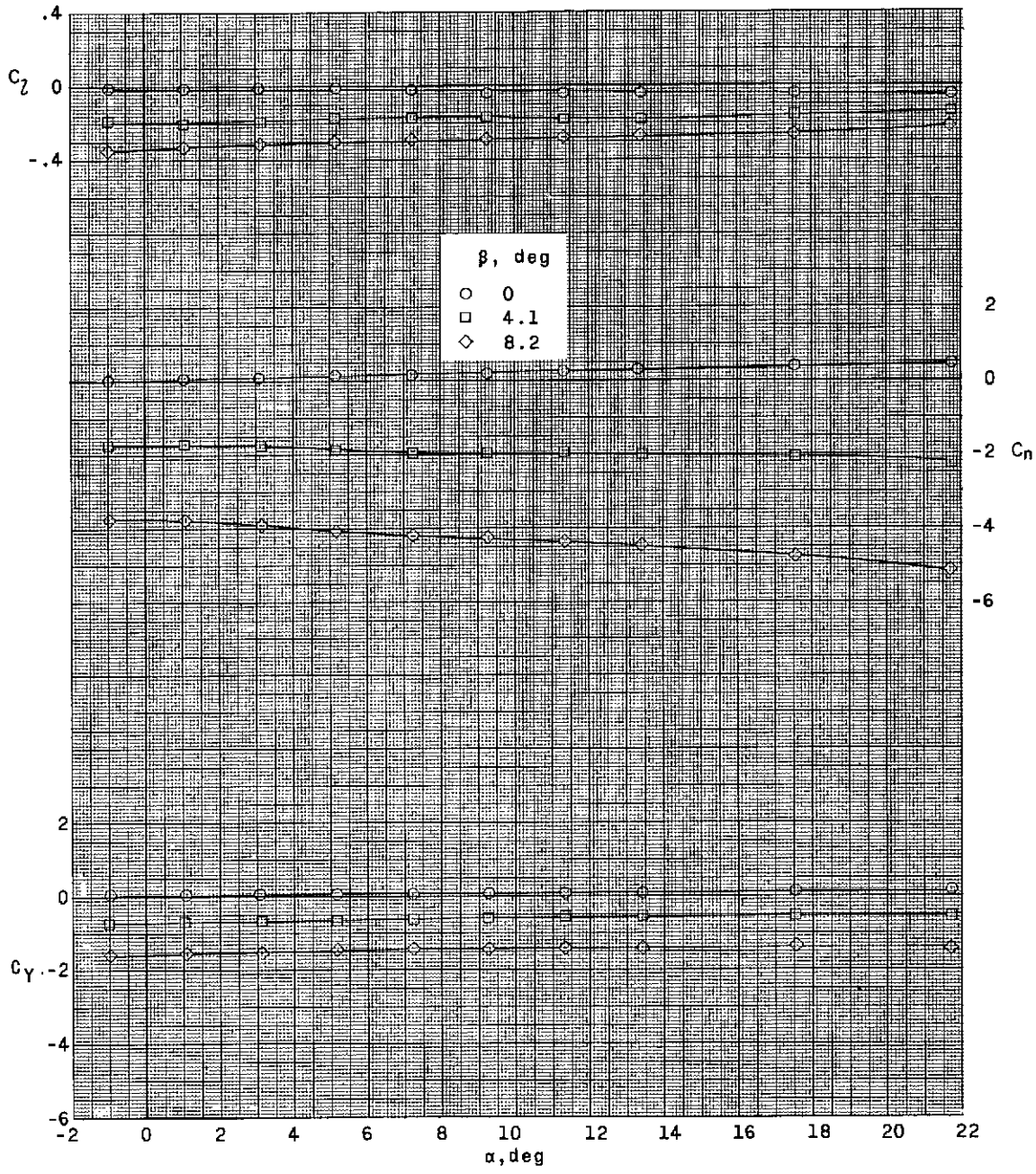

(c) $\delta_e = 20.0^\circ$; $\delta_r = \delta_a = 0^\circ$. Concluded.

Figure 7.- Concluded.

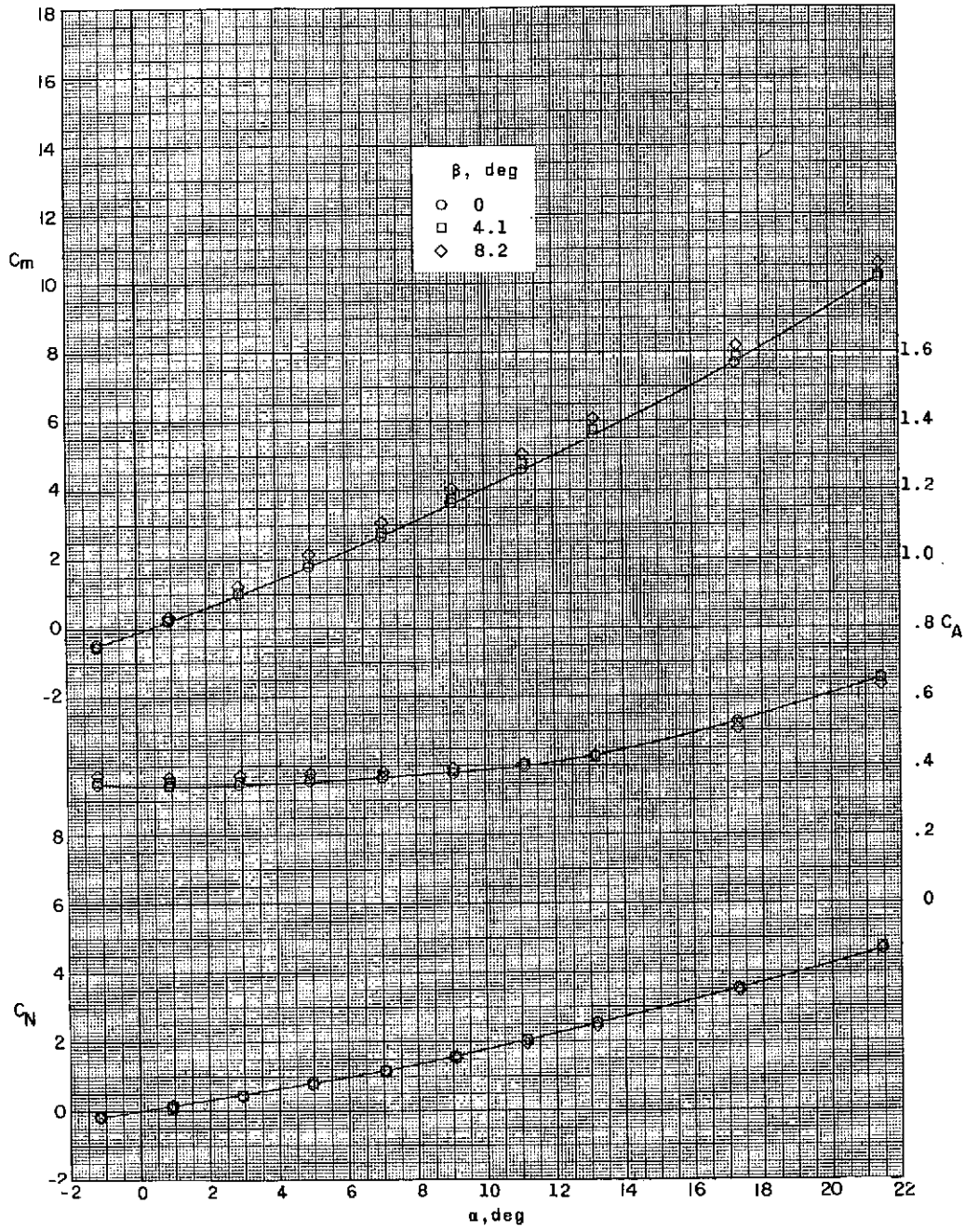

(a) $\delta_e = 0^\circ$; $\delta_r = \delta_a = 0^\circ$; with flared skirt.

Figure 8.- Effect of pitch and differential control deflection on aerodynamic characteristics of model with small canard controls.

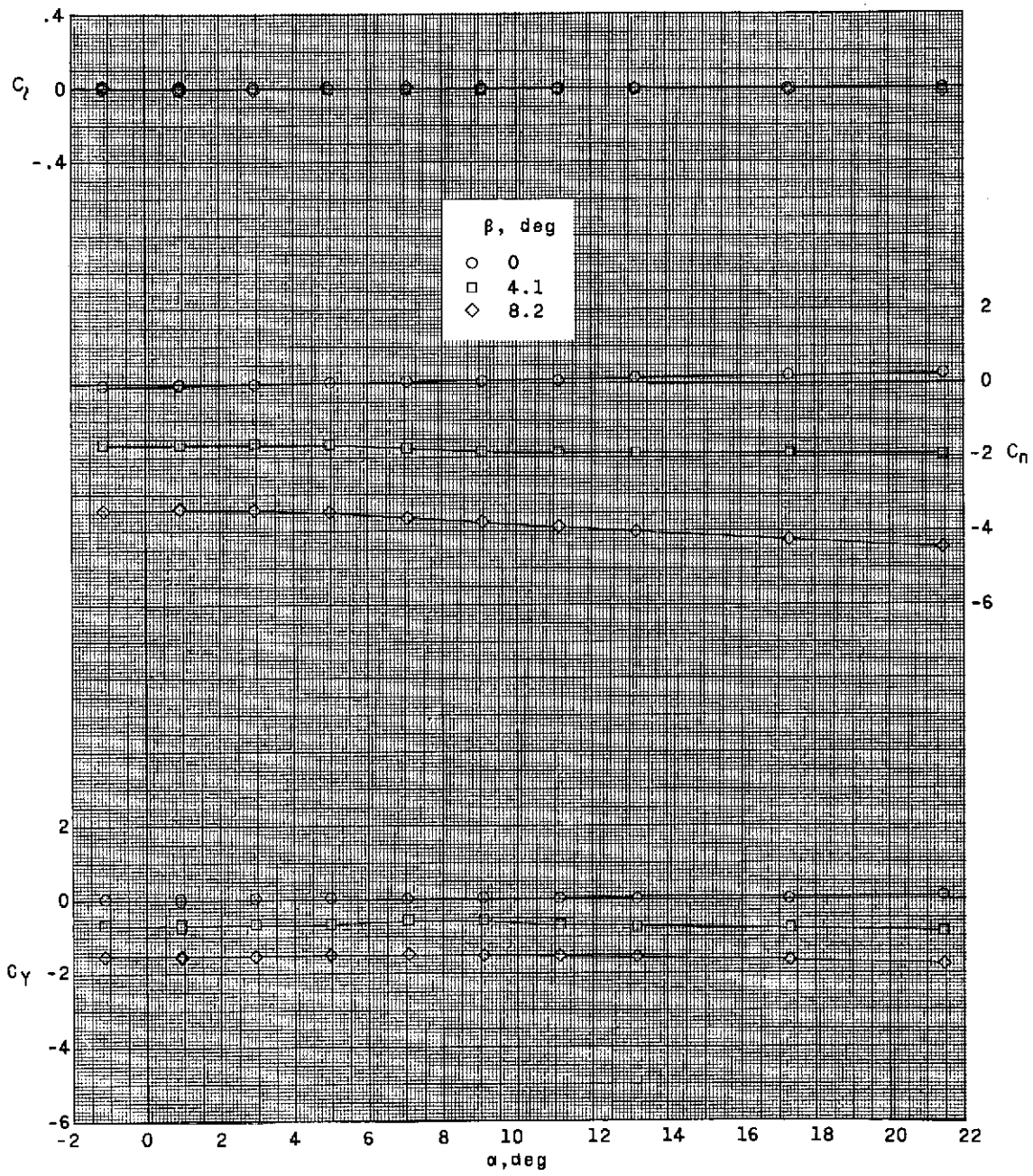

(a) $\delta_e = 0^o$; $\delta_r = \delta_a = 0^o$; with flared skirt. Concluded.

Figure 8.- Continued.

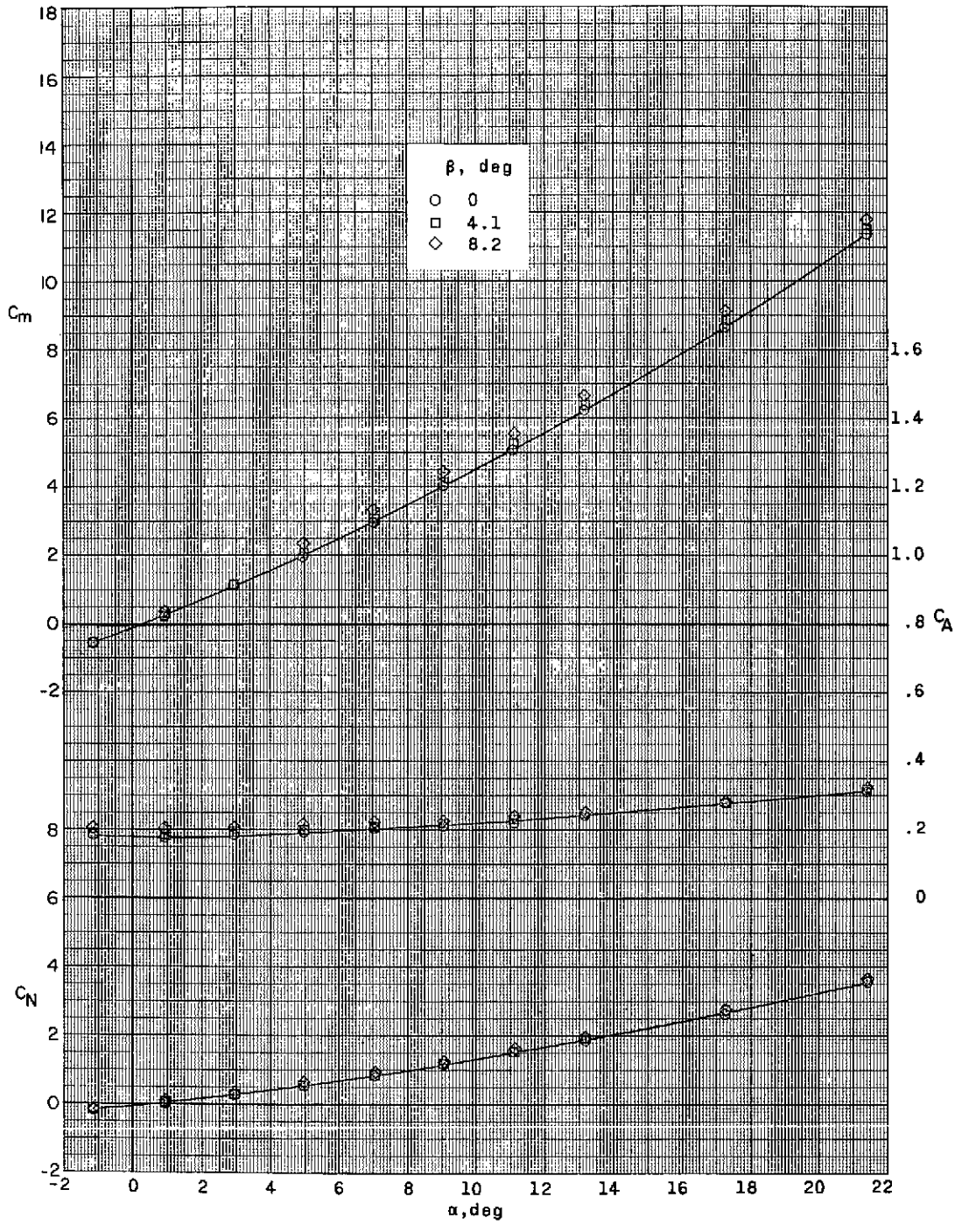

(b) $\delta_e = 0^o$; $\delta_r = \delta_a = 0^o$; without flared skirt.

Figure 8.- Continued.

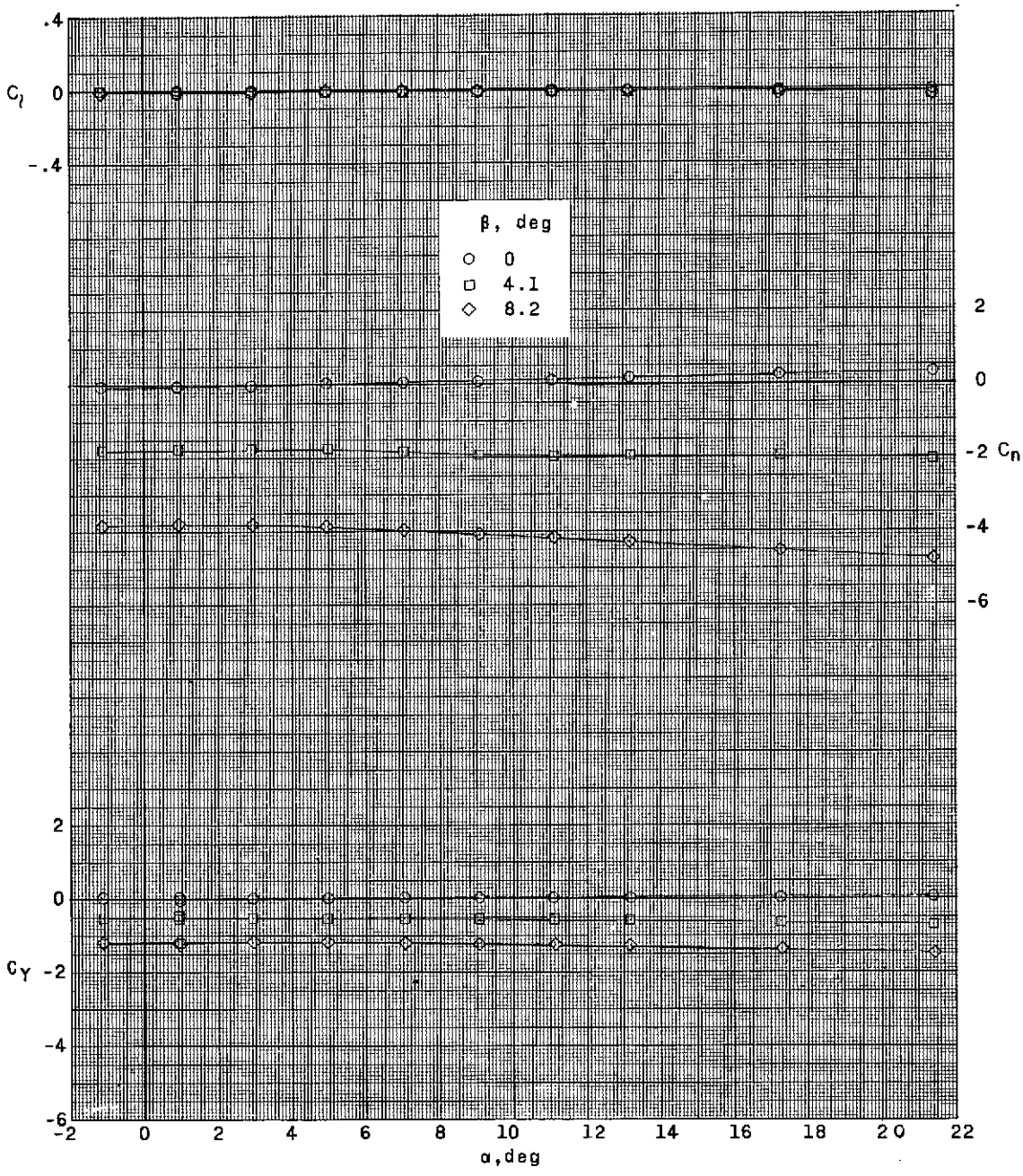

(b) $\delta_e = 0^o$; $\delta_r = \delta_a = 0^o$; without flared skirt. Concluded.

Figure 8.- Continued.

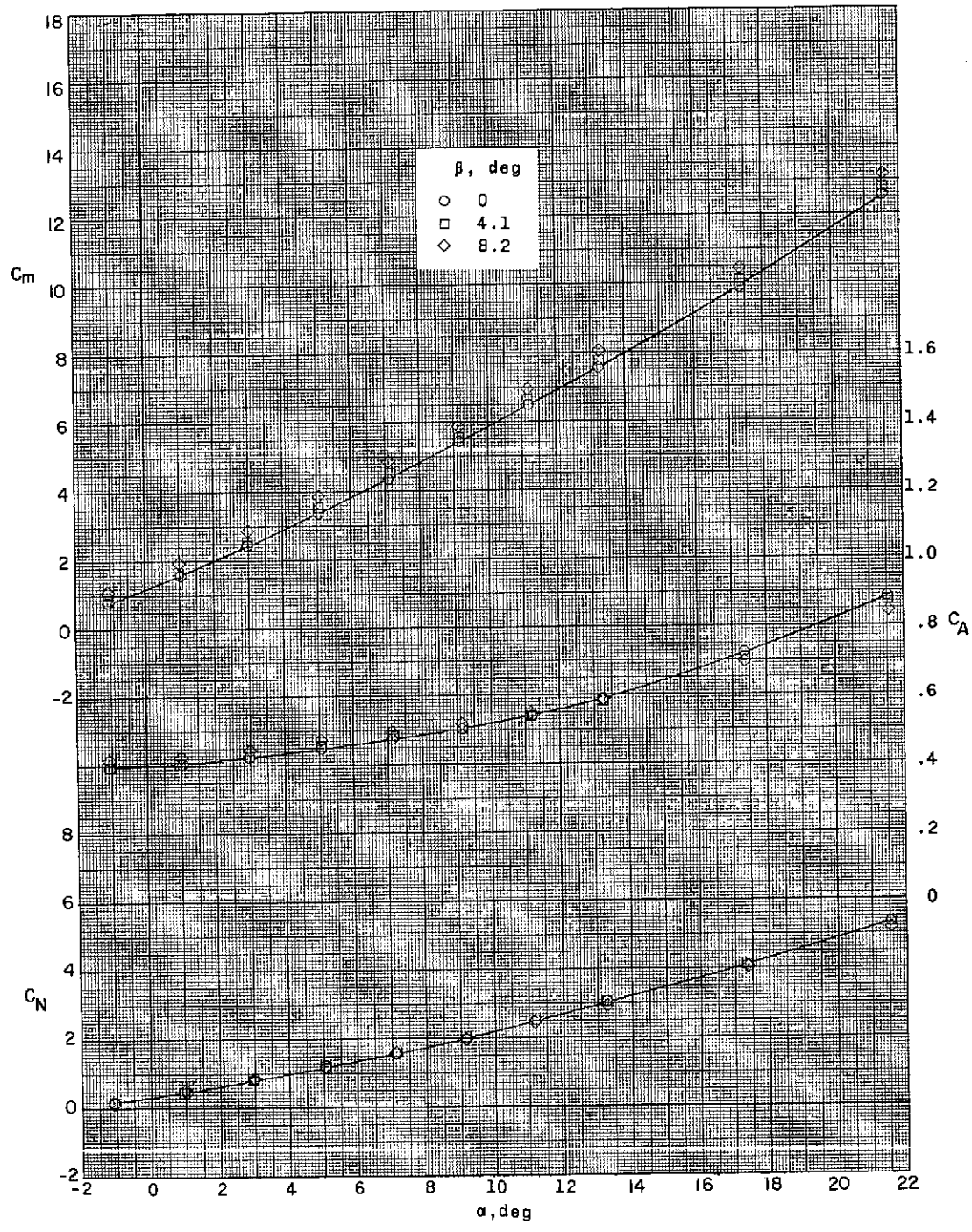

(c) $\delta_e = 10.0^\circ$; $\delta_r = \delta_a = 0^\circ$; with flared skirt.

Figure 8.- Continued.

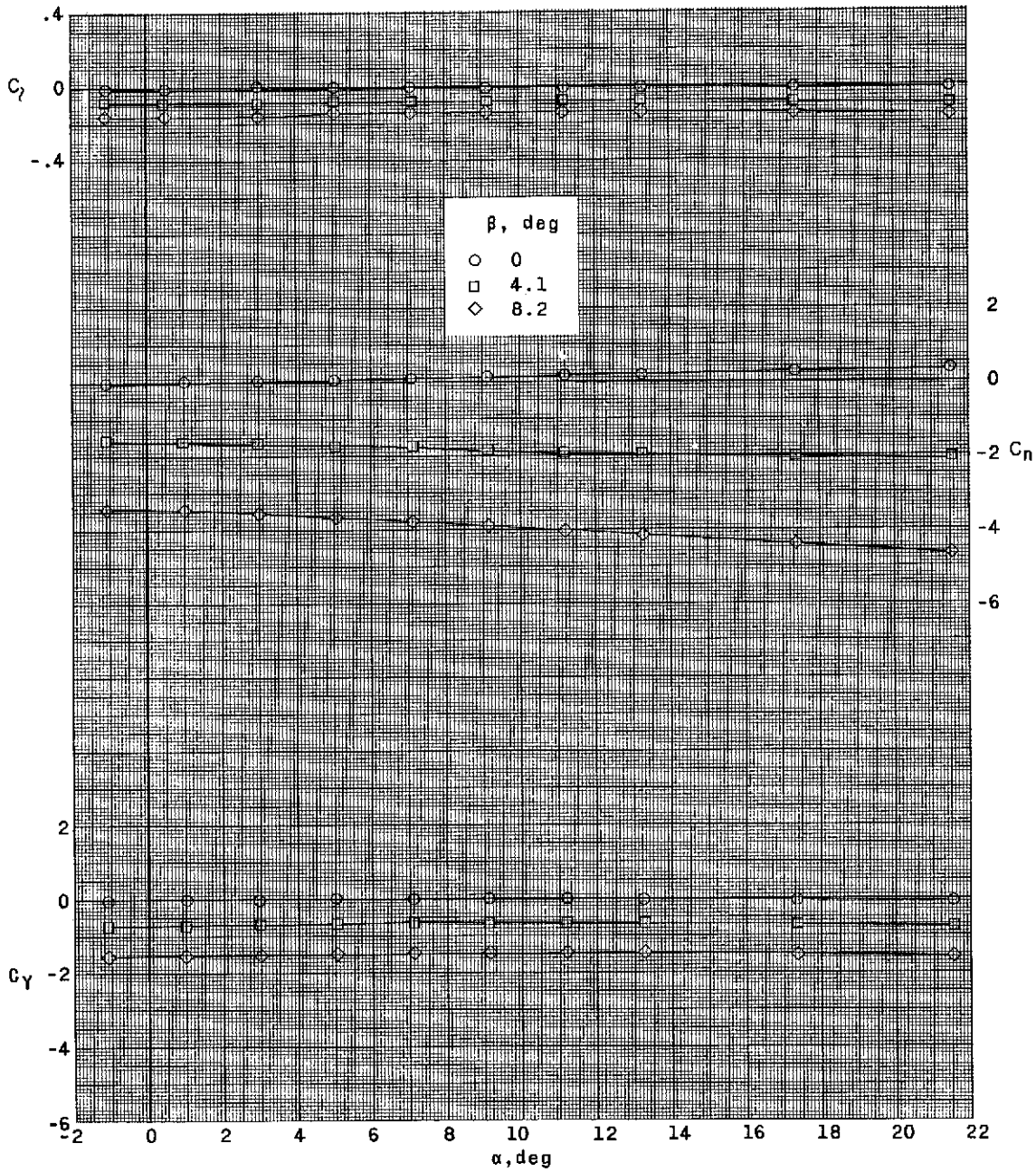

(c) $\delta_e = 10.0^\circ$; $\delta_r = \delta_a = 0^\circ$; with flared skirt. Concluded.

Figure 8.- Continued.

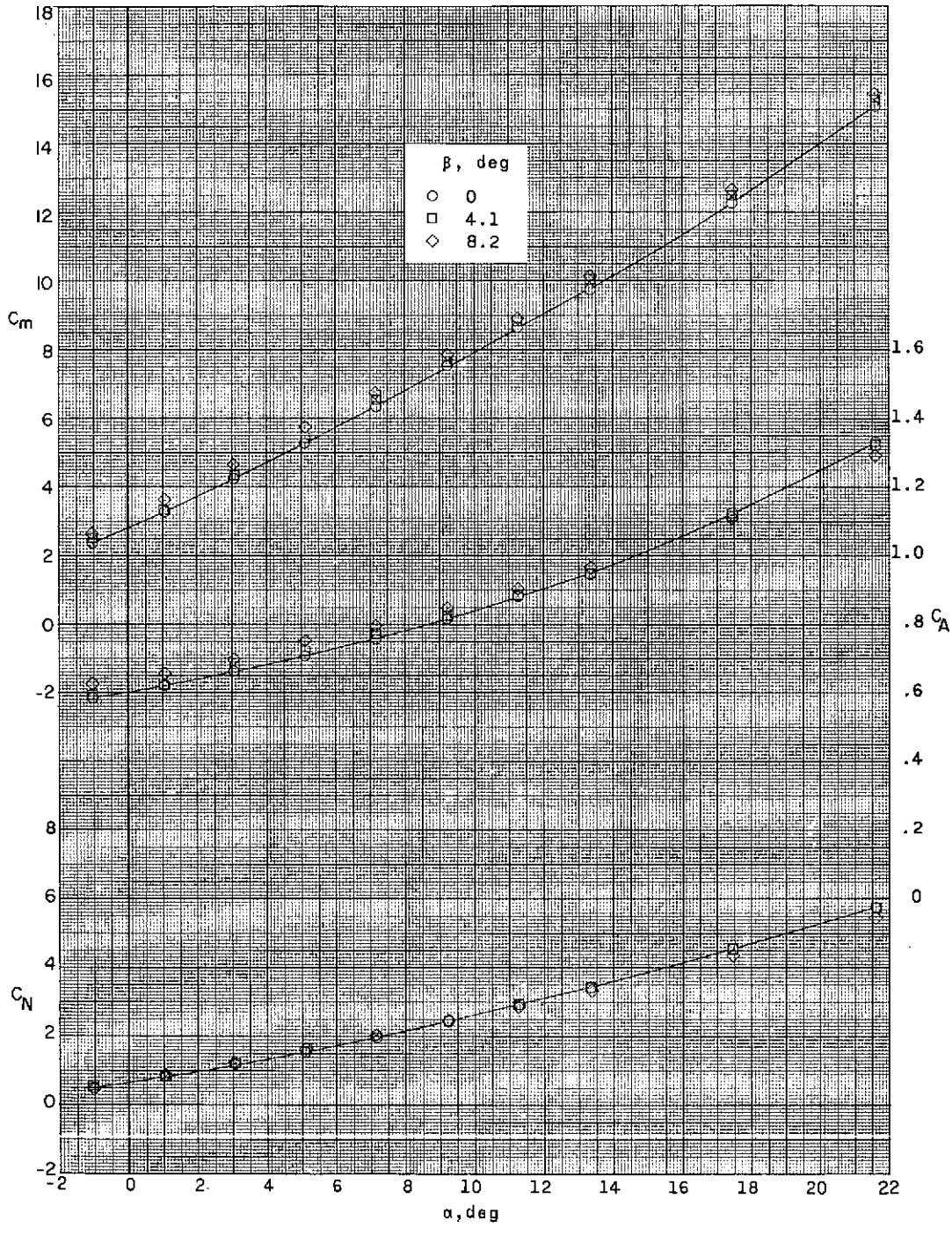

(d) $\delta_e = 20.0^\circ$; $\delta_r = \delta_a = 0^\circ$; with flared skirt.

Figure 8.- Continued.

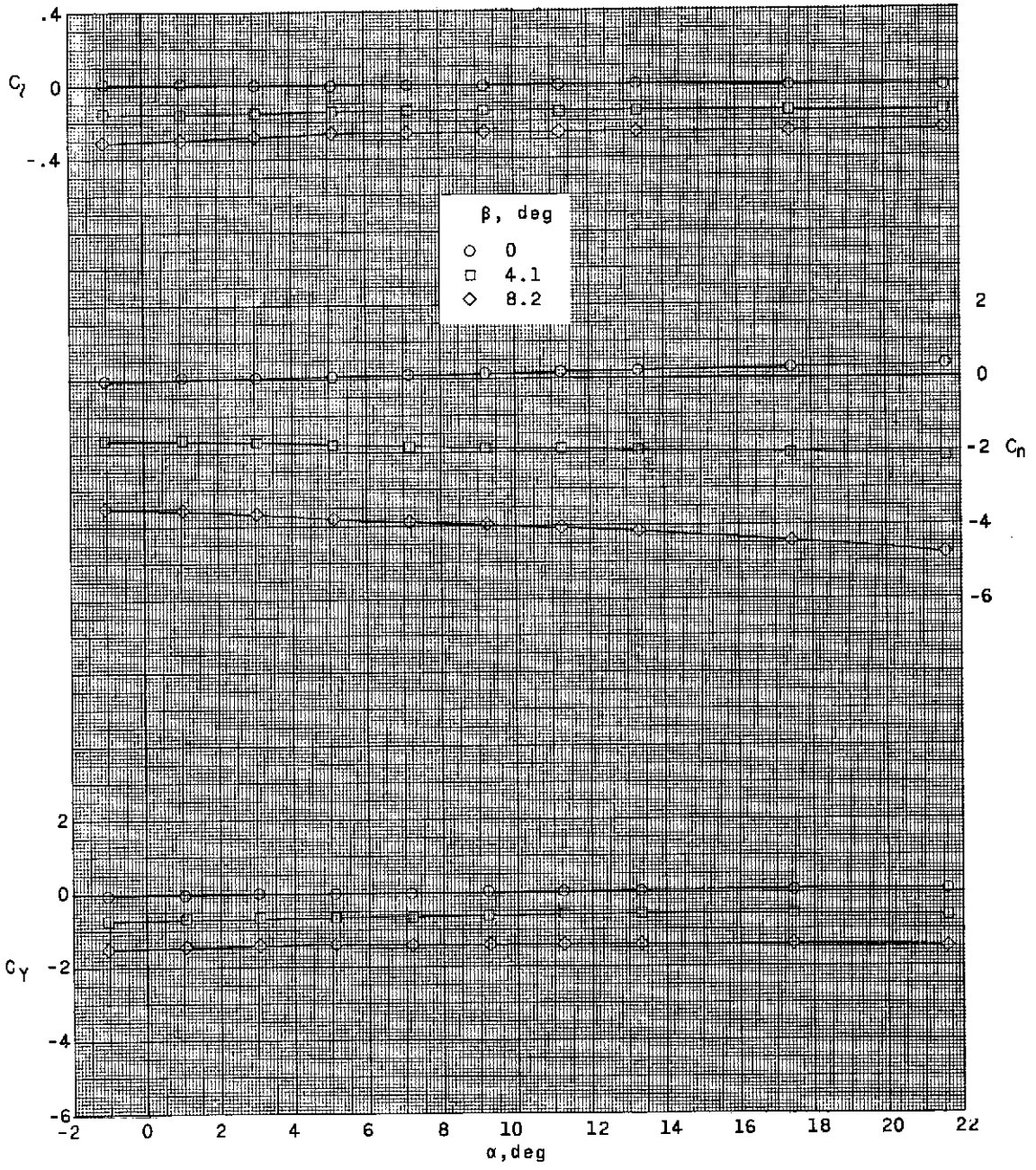

(d) $\delta_e = 20.0^\circ$; $\delta_r = \delta_a = 0^\circ$; with flared skirt. Concluded.

Figure 8.- Continued.

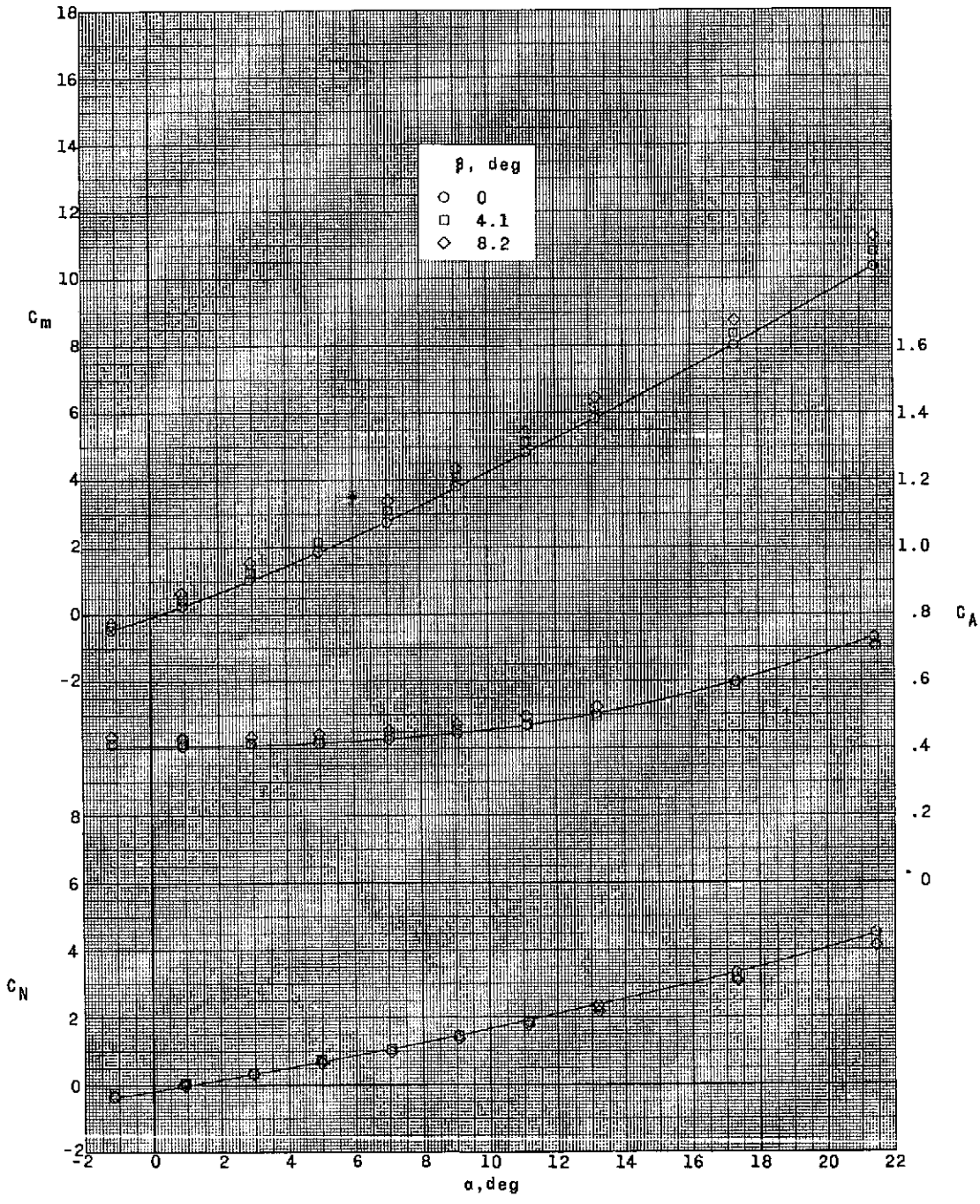

(e) $\delta_a = -20.0^\circ$; $\delta_e = \delta_r = 0^\circ$; with flared skirt.

Figure 8.- Continued.

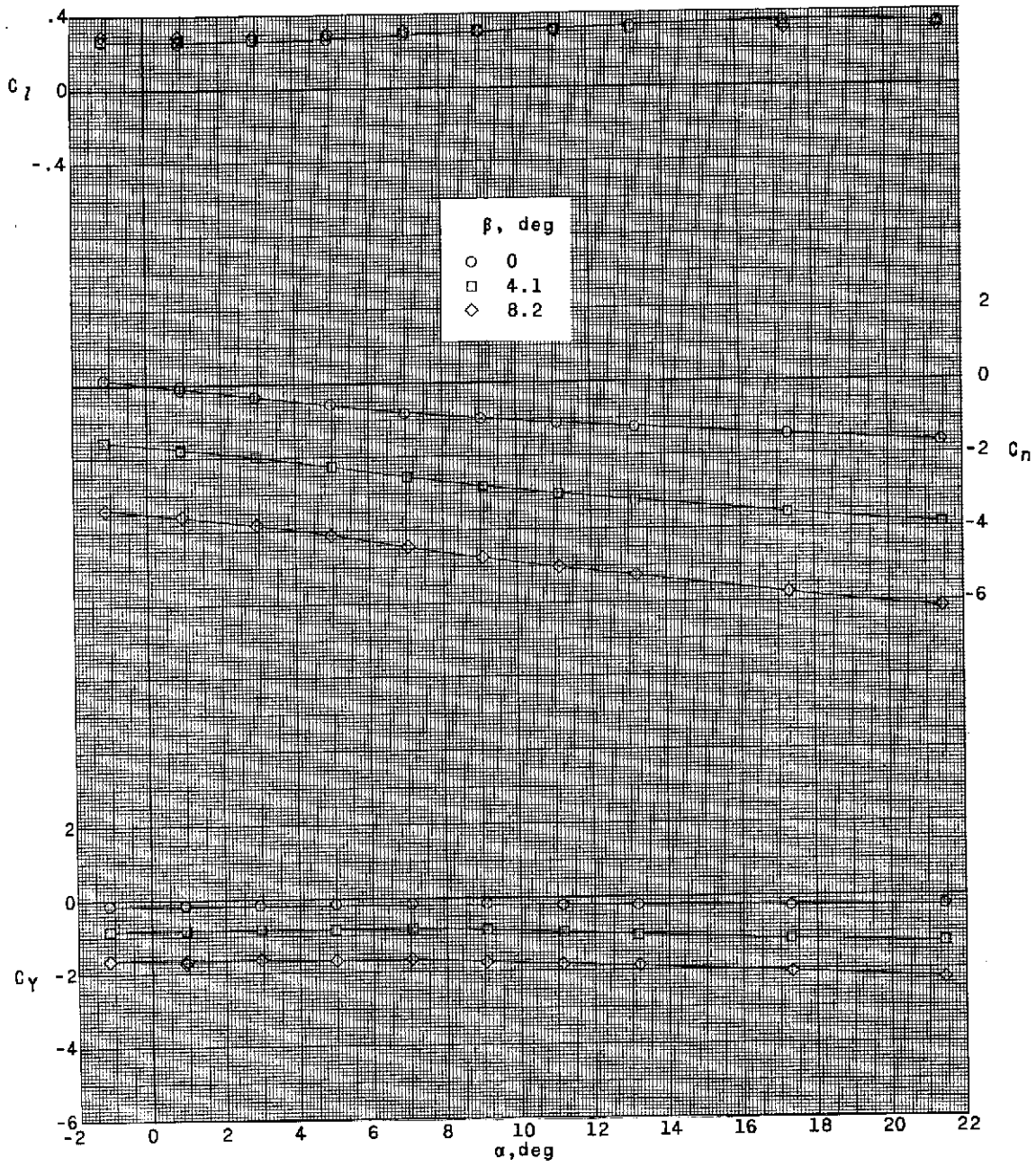

(e) $\delta_a = -20.0^\circ$; $\delta_e = \delta_r = 0^\circ$; with flared skirt. Concluded.

Figure 8.- Concluded.

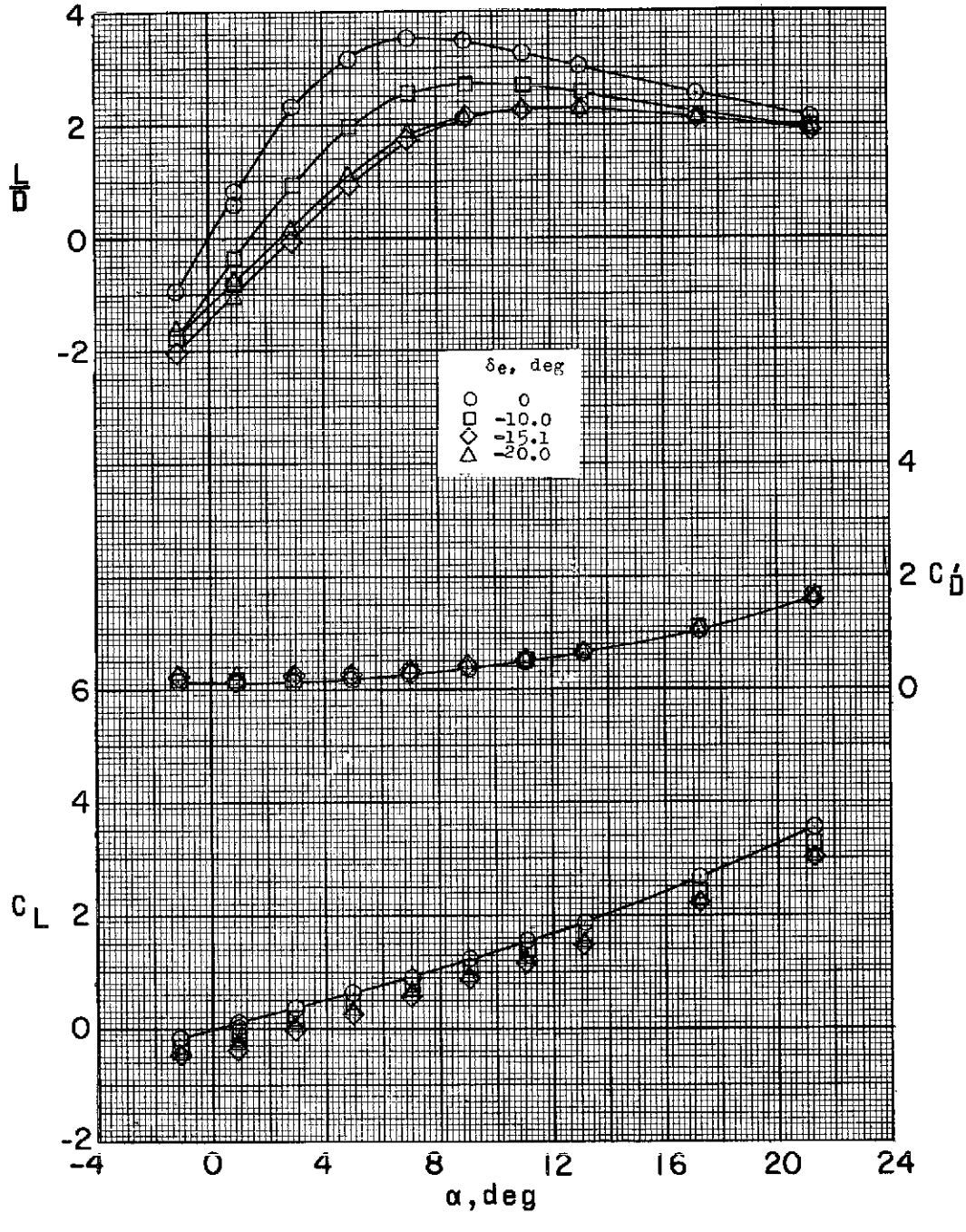

(a) Model with delta fins and trailing-edge controls.

Figure 9.- Effect of pitch control deflection and flared skirt on aerodynamic characteristics about stability axes. $\beta = 0^{o}$.

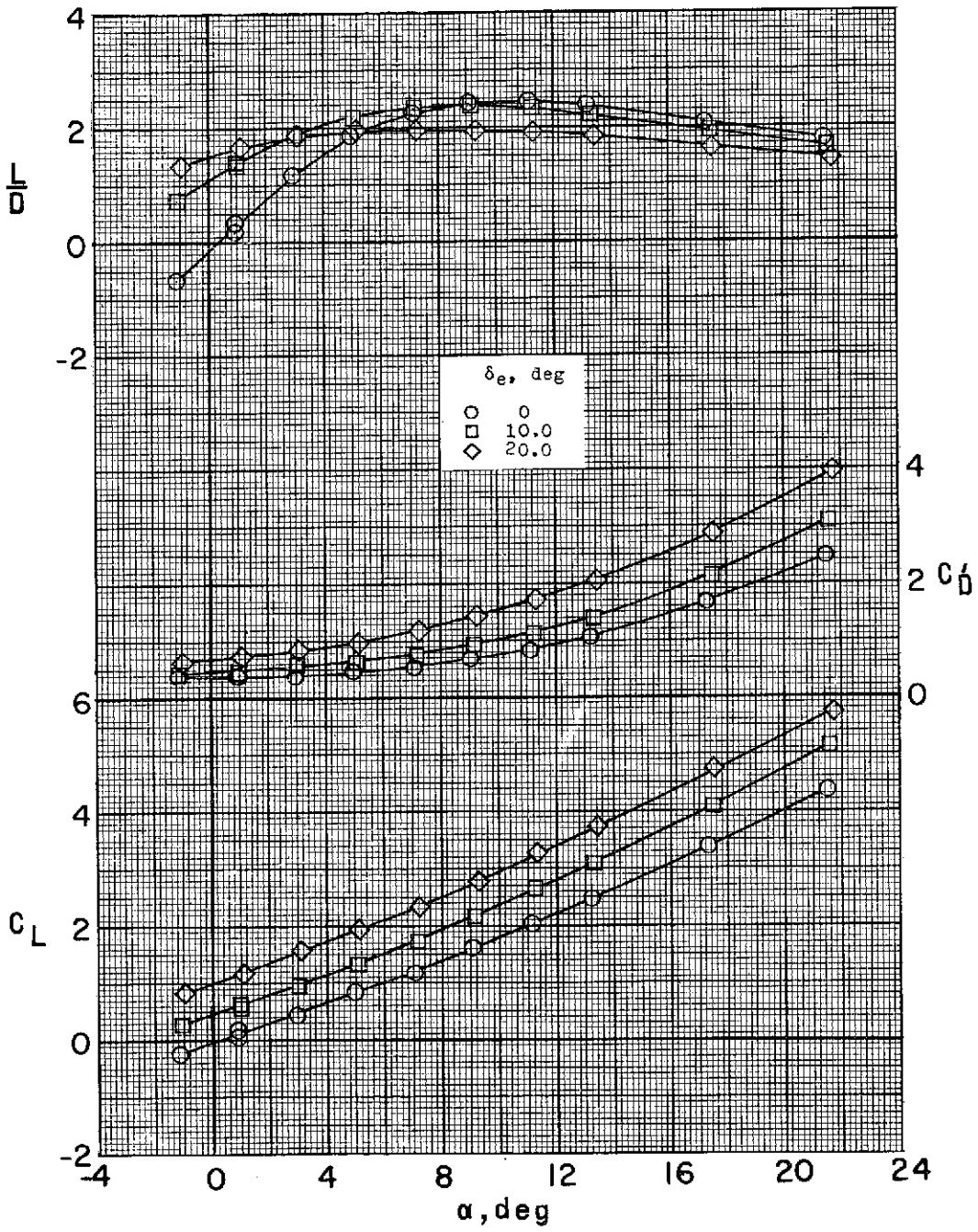

(b) Model with flared skirt and large canard controls.

Figure 9.- Continued.

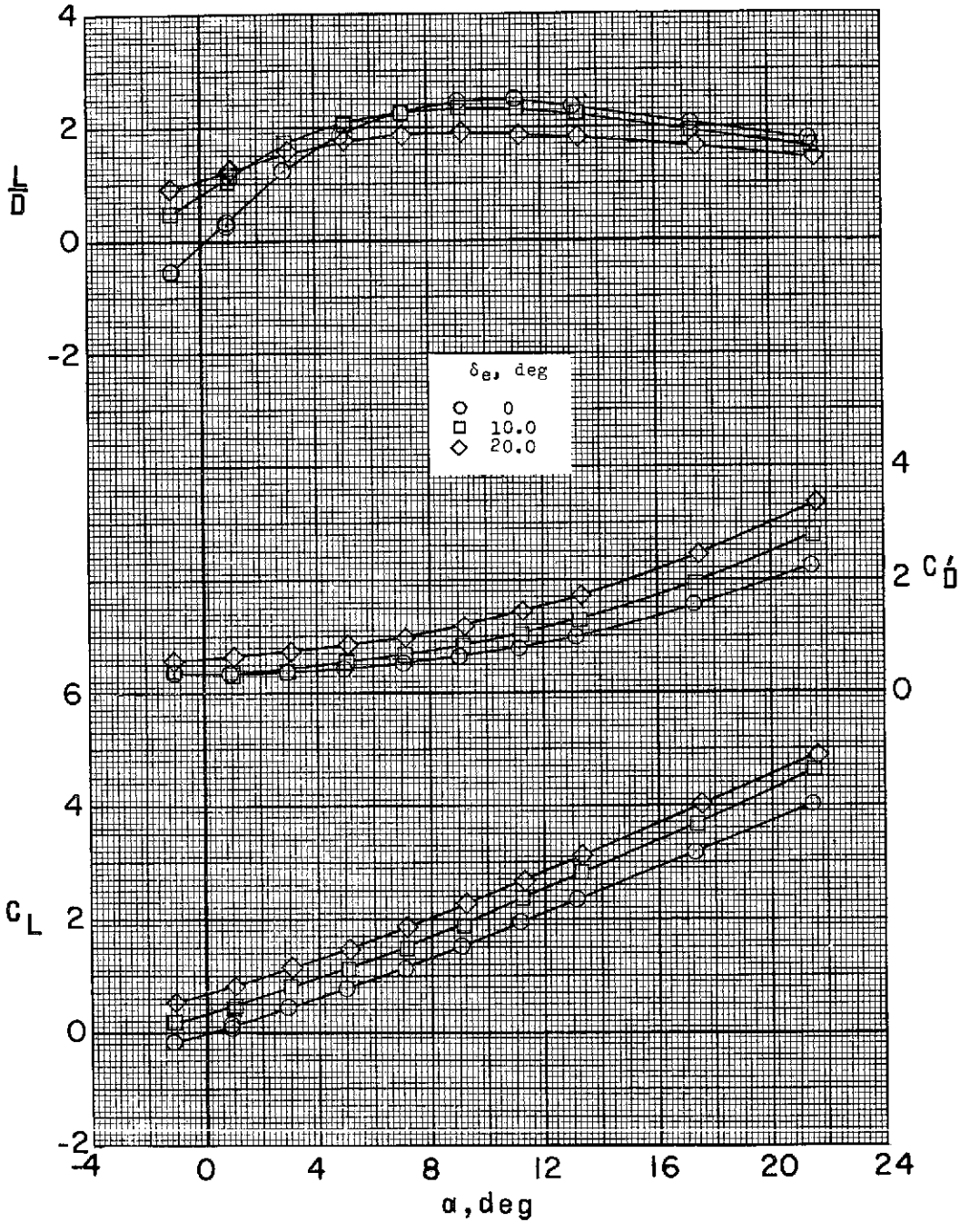

(c) Model with flared skirt and small canard controls.

Figure 9.- Continued.

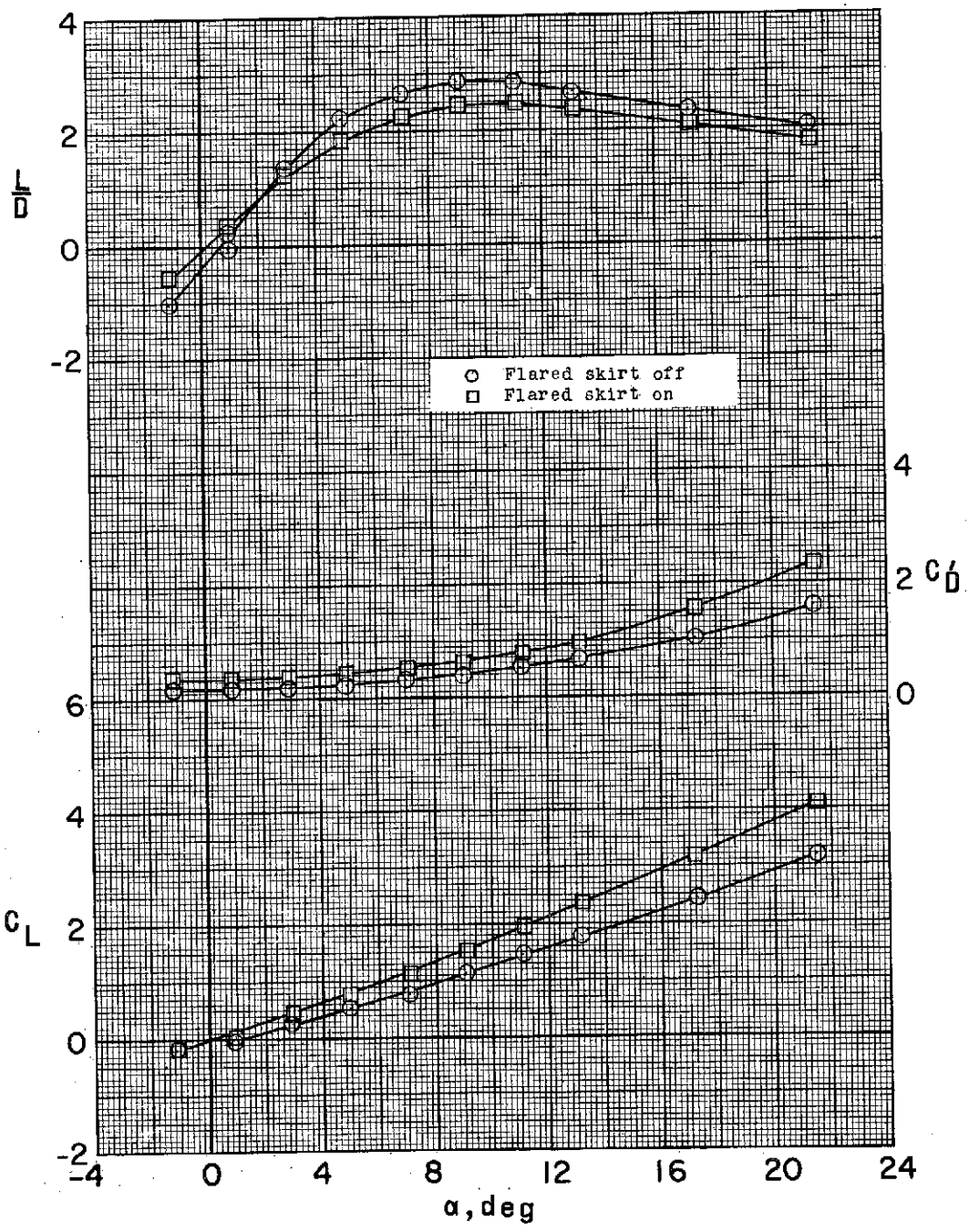

(d) Model with small canard controls.

Figure 9.- Concluded.

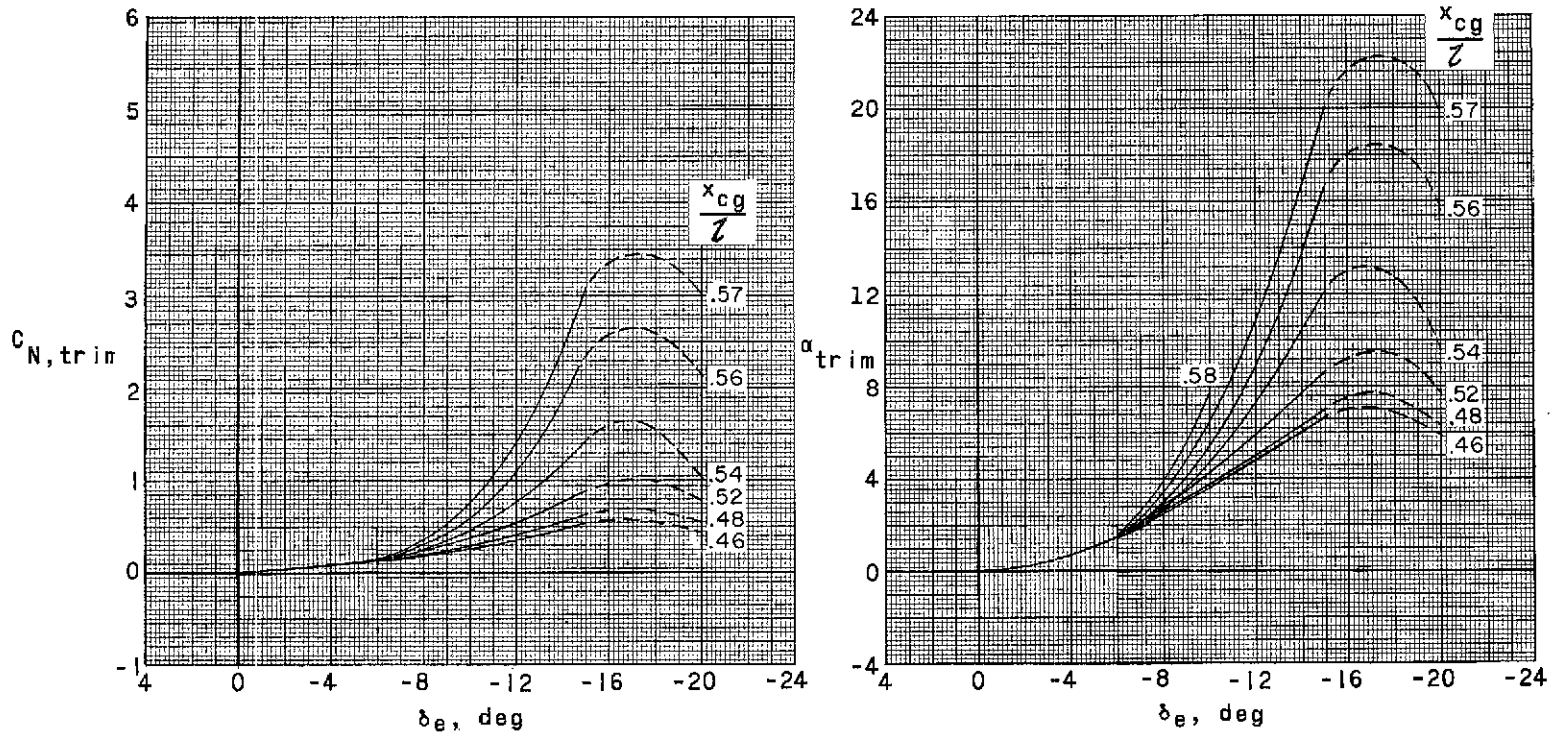

(a) Model with delta fins and trailing-edge controls. Dashed lines indicate unknown variations.

Figure 10.- Effect of center-of-gravity location on trim effectiveness of the various controls. $\beta = 0^{\circ}$.

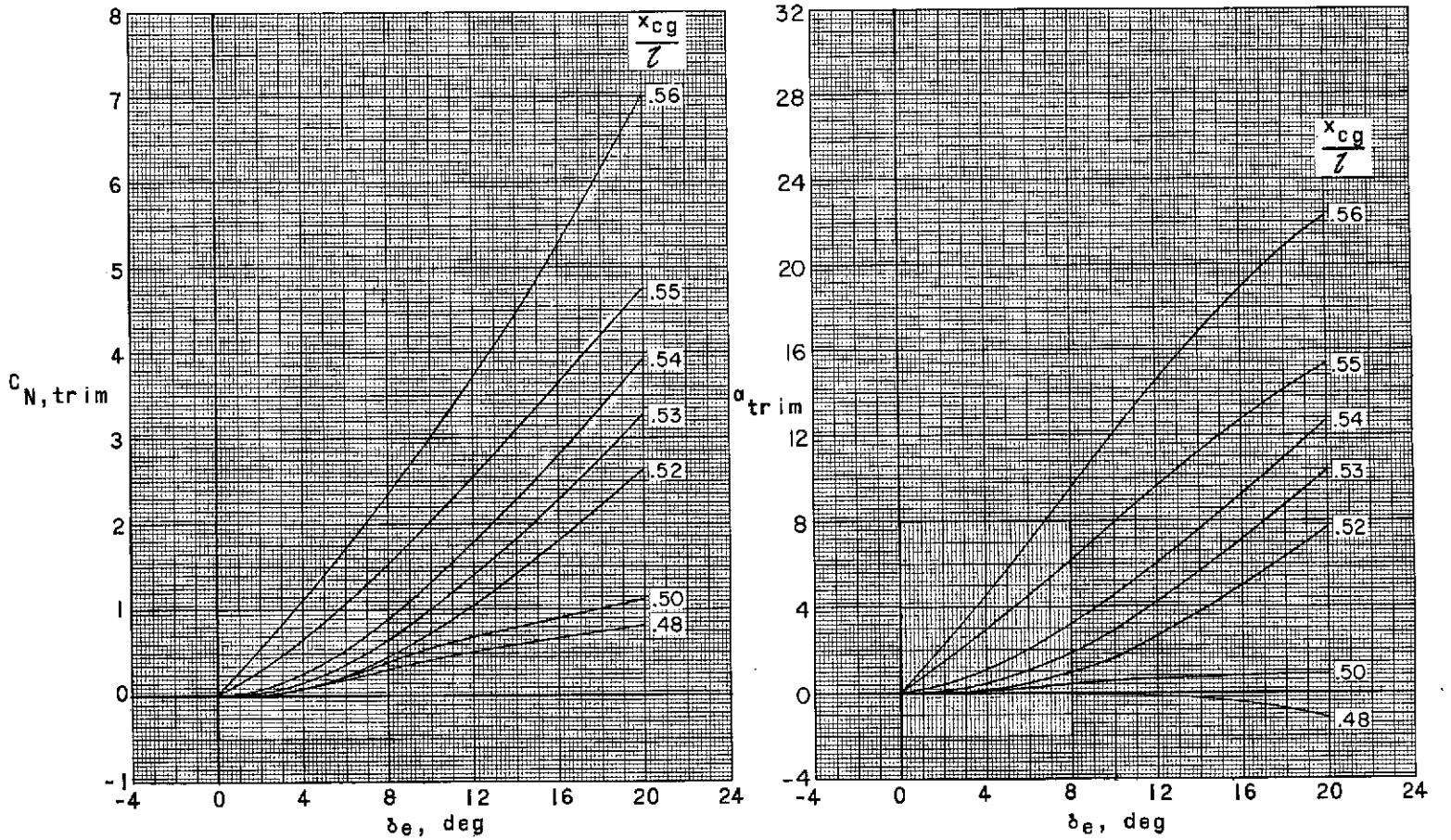

(b) Model with flared skirt and large canard controls.

Figure 10.- Continued.

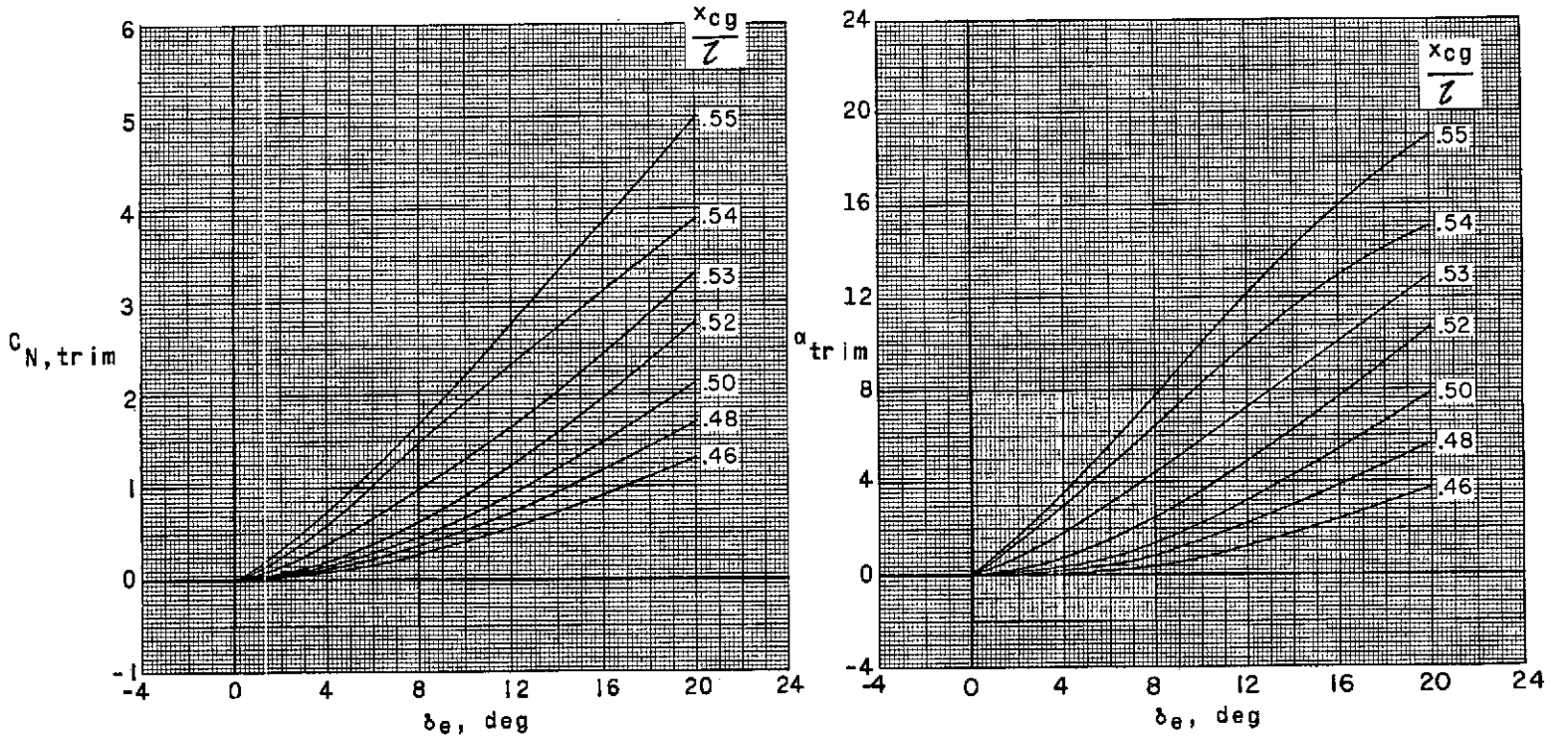

(c) Model with flared skirt and small canard controls.

Figure 10.- Concluded.

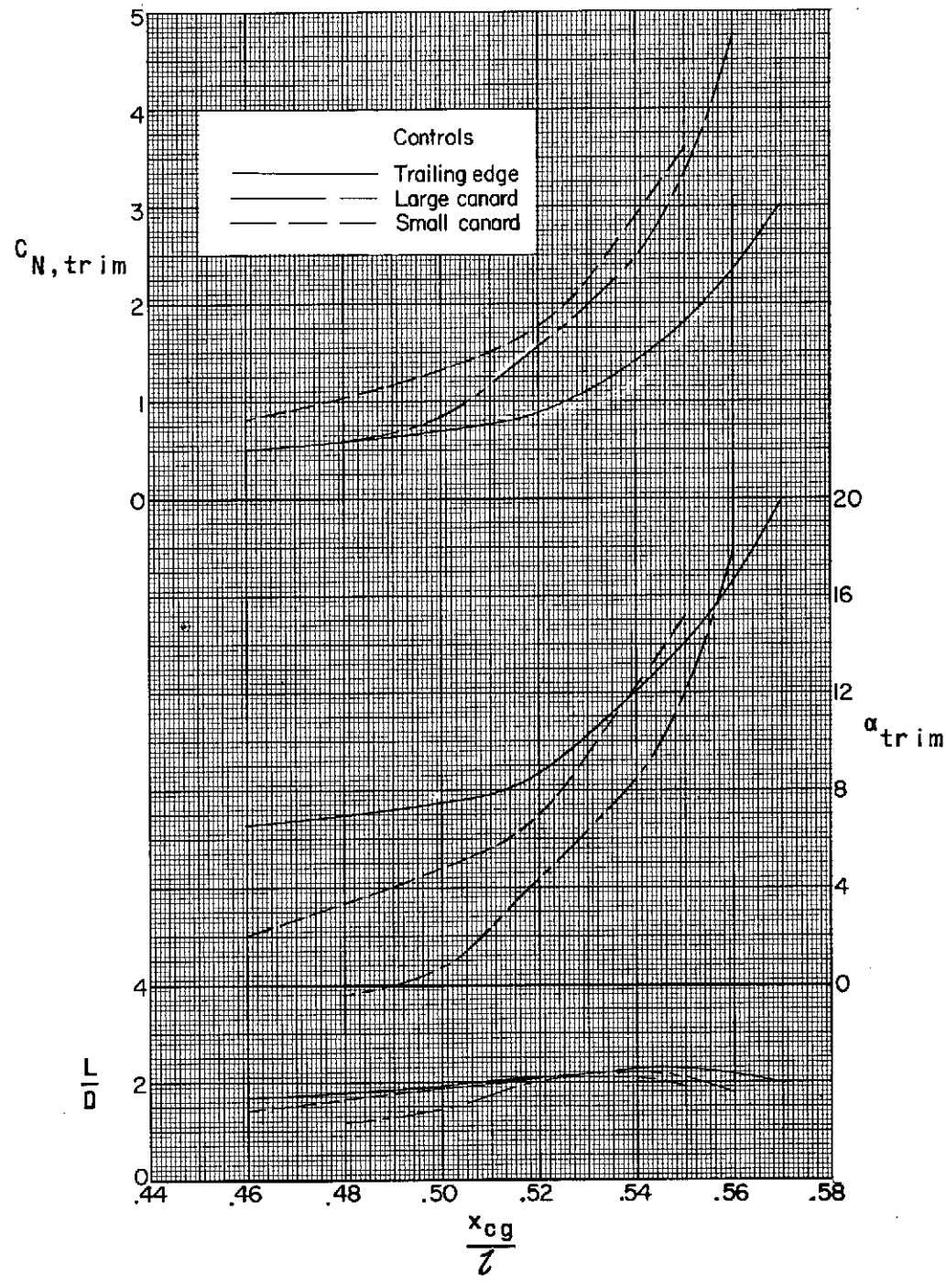

Figure 11.- Comparison of the trim characteristics of various control arrangements. $|\delta_e| = 15.0^\circ$.

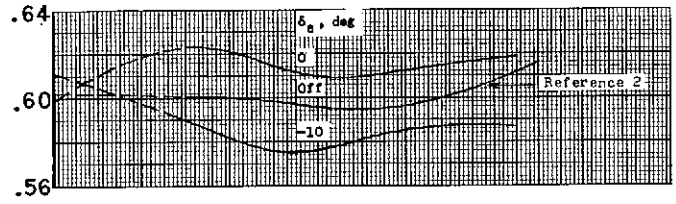

(a) Trailing-edge controls (delta fins).

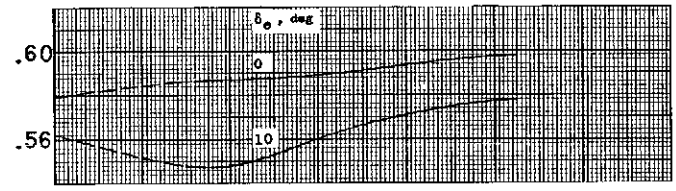

(b) Large canard control (flare on).

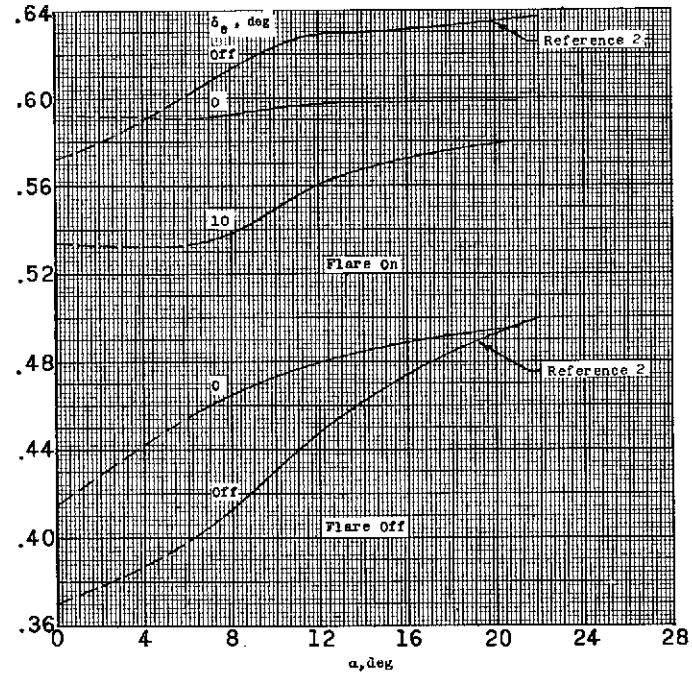

(c) Small canard control.

Figure 12.- Variation of longitudinal center-of-pressure location with angle of attack. $\beta = 0^{\circ}$. Dashed portion of curve indicates center-of-pressure values determined by slopes.

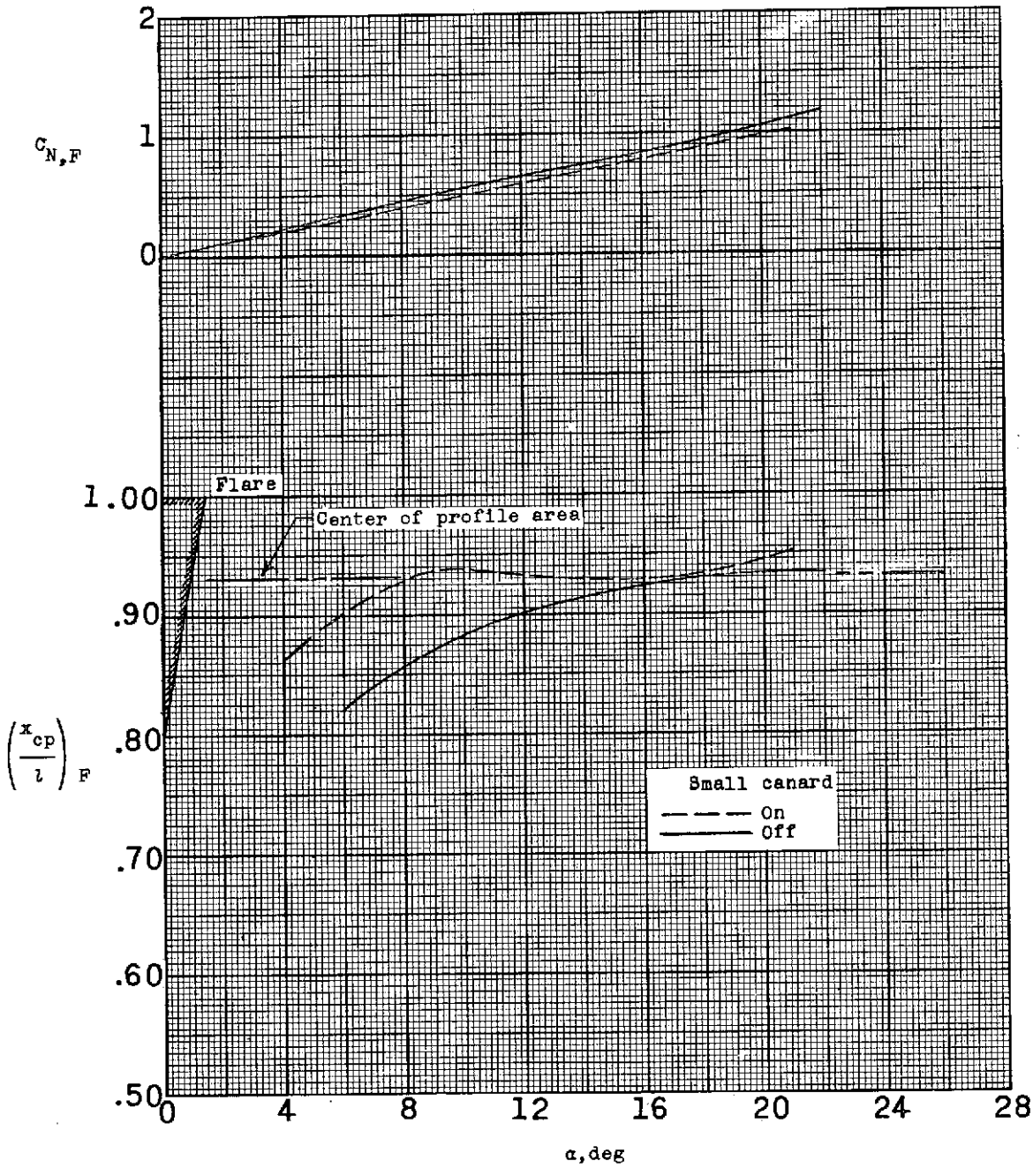

Figure 13.- Effect of canard control on pitch characteristics of flared skirt in presence of body. $\beta = 0^{\circ}$.

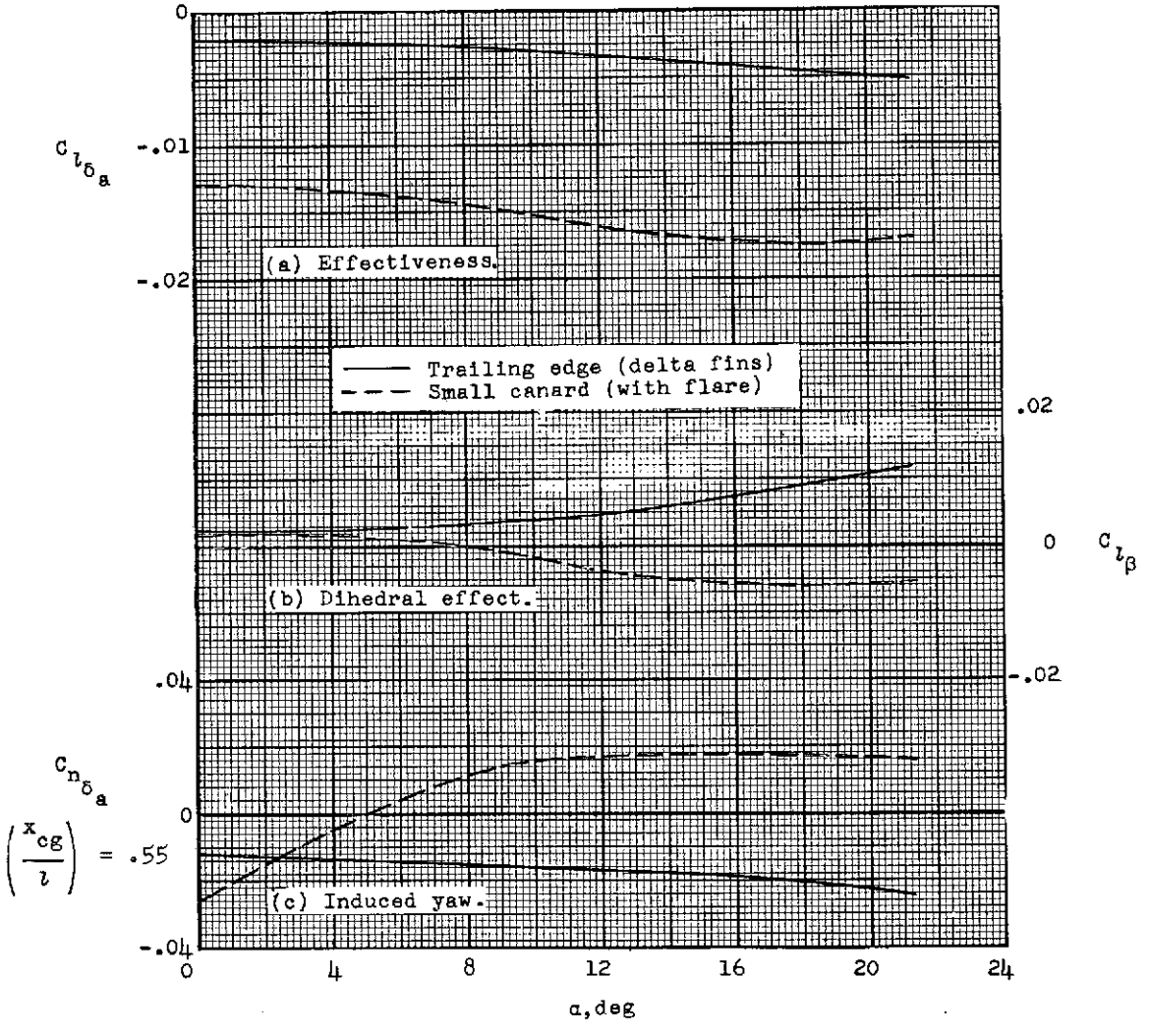

Figure 14.- Effect of angle of attack on aileron characteristics of models. $\beta \approx 0^{\circ}$.

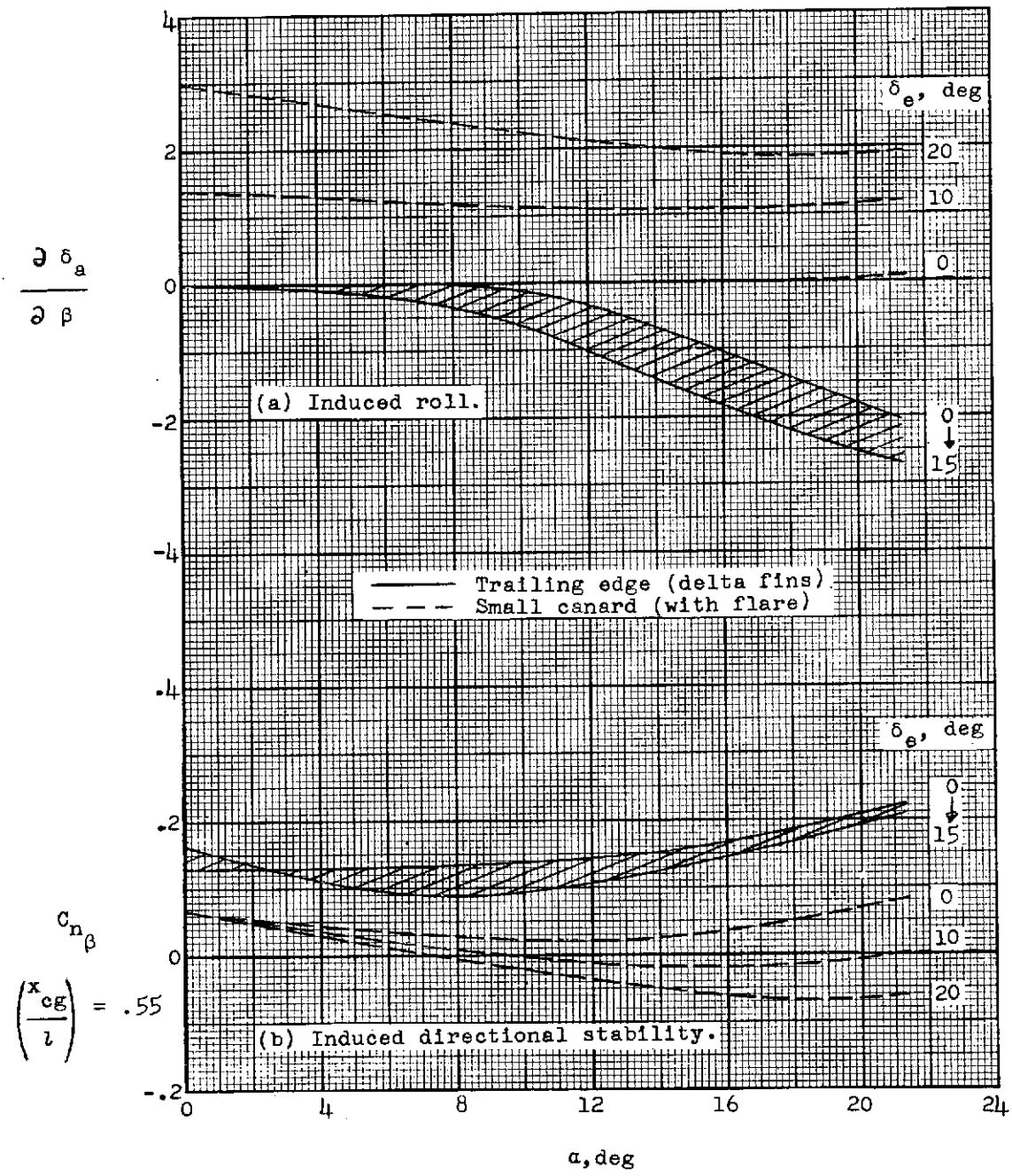

Figure 15.- Effect of pitch control deflection on induced lateral characteristics of two of the models.